To the Graduate Council:

I am submitting herewith a thesis written by Manfred Kurt Kopp entitled "Position-Sensitive Proportional Counters Using Resistance-Capacitance Position Encoding." I recommend it be accepted in partial fulfillment of the requirements for the degree of Master of Science, with a major in Electrical Engineering.

T. V. Blalock, Major Professor

We have read this thesis and recommend its acceptance:

Accepted for the Council:

Vice Chancellor
Graduate Studies and Research

POSITION-SENSITIVE PROPORTIONAL COUNTERS USING RESISTANCE-CAPACITANCE POSITION ENCODING

A Thesis

Presented for the

Master of Science

Degree

The University of Tennessee

Manfred Kurt Kopp

June 1975

ACKNOWLEDGEMENT

This research was performed at the Oak Ridge National Laboratory under the sponsorship of the United States Atomic Energy Commission under contract with the Union Carbide Corporation.

The author wishes to express his sincere appreciation to C. J. Borkowski, Director of the Instrumentation and Controls Division, for suggesting the original idea of RC position encoding and for his guidance, supervision, and assistance in implementing this work.

The author gratefully acknowledges the guidance and encouragement of T. V. Blalock who served as his major professor.

For his continuous interest and assistance and for many helpful suggestions and stimulating discussions, the author thanks C. H. Nowlin of ORNL; and for their assistance in constructing the experimental PSPCs the author is grateful to J. A. Williams, R. E. Zedler, C. E. Fowler, and G. W. Allin, all of ORNL.

The author appreciates the assistance of Mrs. Vivian Zedler of ORNL in the preparation of this thesis.

1297194

ABSTRACT

A new method was developed for encoding the position of individual photons, neutrons, or charged particles in proportional counters by using the distributed RC line characteristics of these counters. The signal processing is described and guidelines for the design and operation of these position sensitive proportional counters (PSPCs) are given.

Using these guidelines, several prototypic PSPCs were constructed to improve the spatial resolution and shorten the signal processing time; for example, the intrinsic spatial uncertainty was reduced to 28 μ fwhm for alpha particles and 100 μ fwhm for low-energy x rays (2 to 6 keV). Also, the signal processing time was reduced to 0.6 μsec without seriously degrading the spatial resolution.

These results have opened new fields of application of the RC position encoding method in imaging distributions of photons, charged particles, or neutrons in nuclear medicine, physics, and radiography.

TABLE OF CONTENTS

CHAPTER		PAGE
I.	INTRODUCTION	1
II.	DESCRIPTION OF POSITION-SENSITIVE PROPORTIONAL COUNTERS USING RC-ENCODING	3
	Line Counters	3
	Area Counters	7
III.	ENERGY LOSS, DETECTION TIME, AND POSITION OF A SINGLE IONIZING EVENT	13
IV.	SIGNAL PROCESSING FOR A SINGLE IONIZING EVENT	18
	RC-Encoding of Position, Energy Loss, and Detection Time	18
	Position Decoding	23
	Energy-Loss Decoding	30
	Detection-Time Decoding	31
	Description of the Signal Processing Circuit	31
V.	SOURCES OF SPATIAL UNCERTAINTY	37
	Thermal Noise	38
	Drift Field Distortion	40
	Detection Process	42
	Charged particles	42
	Thermal neutrons	43
	Low-energy photons	45
	Source Position	46
VI.	ERRORS IN THE MEASUREMENT OF ENERGY LOSS AND DETECTION TIME	48

CHAPTER PAGE

VII. MEASUREMENT RESULTS 53

Spatial Uncertainty for Alpha Particles and X Rays . . . 53

Position-Signal Processing Time 57

Count-Rate Capability 59

VIII. APPLICATIONS 62

IX. CONCLUSIONS 64

LIST OF REFERENCES 67

VITA 71

LIST OF FIGURES

FIGURE		PAGE
1.	Construction Details of a Linear Position-Sensitive Proportional Counter Used in Laboratory Experiments . . .	4
2.	Diagram of the Principal Steps in the Evolution of an Area PSPC	8
3.	Relation Between the Source Position and the Anode of (a) a Line PSPC and (b) an Area PSPC	15
4.	Circuit Representation of a Distributed RC Line of Finite Length	20
5.	Equivalent Circuit of a Line PSPC of Length L with a Current Source at the Position x	21
6.	Signal Processing Circuit for a Typical Linear PSPC	25
7.	Signal-Flow Diagram for the Time-Difference Analyzer	35
8.	Spatial Distribution of Thermal Neutrons Measured with a Linear PSPC in Response to Two, Collimated and Parallel Neutron Beams, Spaced 1.2 mm, that Intercept the PSPC Perpendicularly to the Anode	44
9.	Measurement Geometry of a Neutron or X-ray Source Position and the Resulting Probabilistic Point Spread Function (Assuming $x_i = x_e$)	47
10.	Approximate Shapes of the Filter Output Signals (a) for the Energy-Loss Measurement and (b) for the Detection-Time Measurement, Represented for Two Event Positions: x = 0 and x = L/2	50
11.	Experimental Counter and Alpha Source Measurement Geometry Showing the Measured Spatial Distribution of Alpha Particles and the Resulting Spatial Uncertainty	55
12.	Spatial Uncertainty as a Function of X-ray Energy Measured with the PSPC of Figure 11, page 55	58

CHAPTER I

INTRODUCTION

A new method was developed using proportional counters to measure the position of sources that emit low-energy photons, neutrons, or charged particles.

Traditionally, gas-filled and semiconductor proportional counters have been used in nuclear physics to measure (1) the energy loss of ionizing events (photons, neutrons or charged particles) in the sensitive volume of the counter, and (2) the time of interaction between the event and the counter materials. In this thesis, a method is presented to extract additional information about the source position from conventional proportional counters. Thus, position-sensitive proportional counters (PSPCs) generate signals that contain information about the position, energy loss, and time of interaction of each detected event.

These PSPCs are useful to image spatial distributions of photons, neutrons, or charged particles in medicine, nuclear physics, materials studies, crystallography, and related areas. In general, the application of PSPCs in these areas has resulted in shorter data acquisition times or lower radiation dose to the subject being imaged compared to conventional imaging techniques such as photography or scanning methods. Other advantages of PSPCs in specific applications are discussed in Chapter VIII.

The development work was limited to the resistance-capacitance (RC) method of position encoding in gas-filled proportional counters.[1-8] Several prototypic PSPCs were built and successfully tested. The results of this work reveal advantages of RC position encoding in many applications over position encoding by signal amplitude division,[9,10] delay lines,[11] or multidetector systems.[12] The main advantages can be summarized as follows: the event position is decoded by time difference measurement, which, in general, is simpler and more reliable than the measurement of signal amplitude ratios; and the detector capacitance is kept as low as possible, which yields low spatial uncertainty without compromising the energy-loss and time resolution inherent of conventional proportional counters.

The description of PSPCs and the RC position encoding method, discussion of signal processing methods and noise sources, and evaluation of test results presented in this thesis have led to the development of approximate models that should serve as guidelines for the design and operation of these devices.

CHAPTER II

DESCRIPTION OF POSITION-SENSITIVE PROPORTIONAL COUNTERS USING RC-ENCODING

Most of this chapter is devoted to a discussion of the modifications required to adapt conventional, gas-filled proportional counters for position encoding by the RC method. Since conventional proportional counters have been discussed extensively in the literature,[13] a description of the construction and characteristics of these counters is beyond the scope of this thesis.

I. LINE COUNTERS

To adapt a conventional, single-anode proportional counter for RC position encoding, both ends of the anode must be accessible as signal output terminals (Figure 1). The anode resistivity and the anode-to-cathode capacitance represent a distributed RC line. The signal transfer characteristics of the two portions of this RC line that are connected between the source position and the two outputs are used to encode the coordinate of the source position. In many cases, the resistivity of the metallic anode of conventional proportional counters is sufficiently high to allow position encoding without modifying the counter.

For example, as shown in "Measurement Results" (Chapter VII), a conventional, 500-mm-long proportional counter with a 7.3 μ diameter,

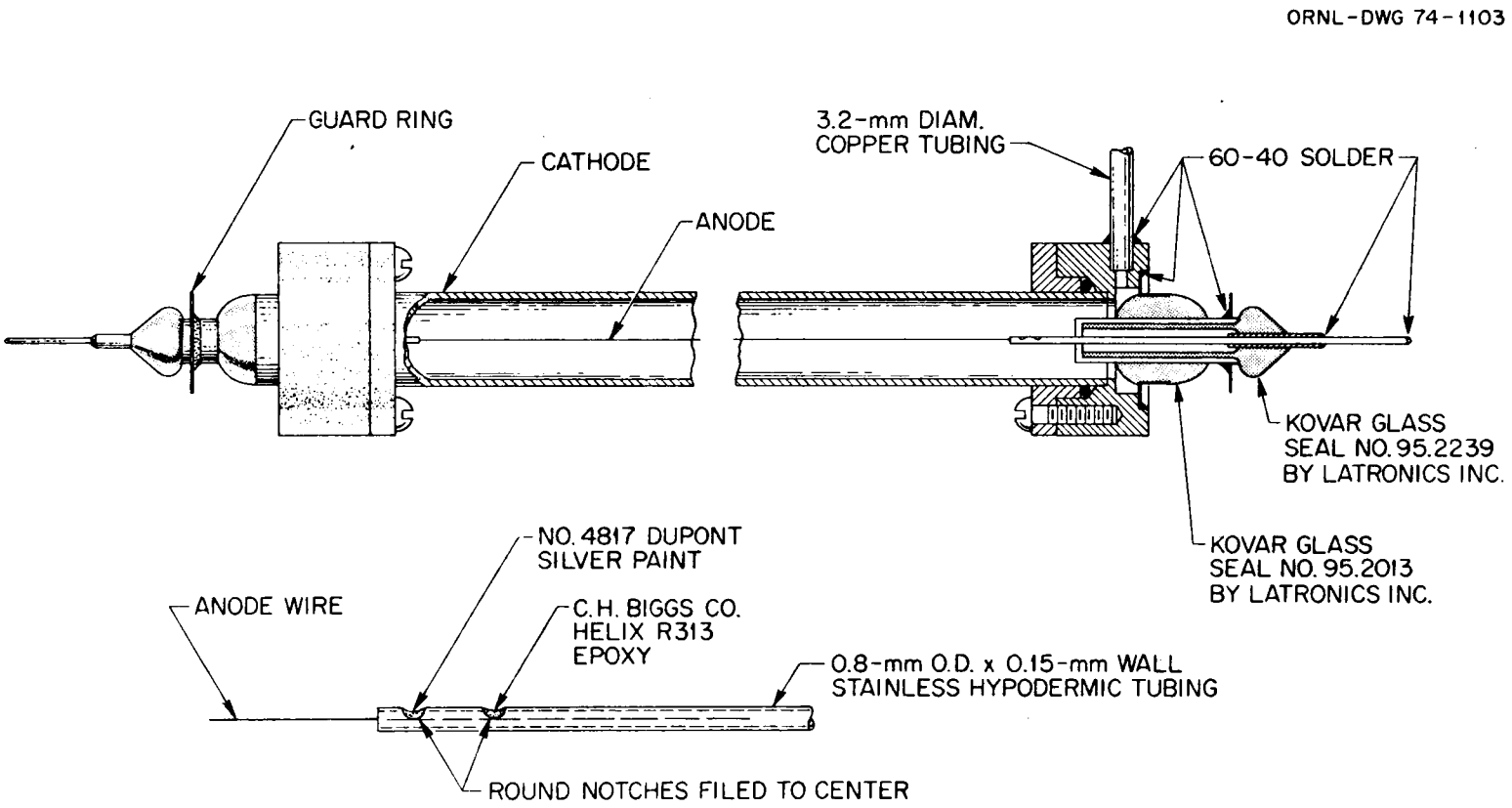


Figure 1. Construction details of a linear position-sensitive proportional counter used in laboratory experiments. (Courtesy of R. E. Zedler, ORNL.)

stainless steel anode wire has sufficient distributed resistance and capacitance to resolve 250 spatial elements. Each position signal requires only 0.55 μs for decoding.

The position decoding time and the counter length can be adjusted independently of the spatial uncertainty by selecting an appropriate value for the anode wire resistivity. A wide range of resistivity values for the anode wires is available to optimize combinations of counter length, spatial resolution, and signal processing times for each application. Table I is a list of available wire materials, dimensions, and resistivities.

For PSPC construction we recommend the same precautions and practices that apply in conventional proportional counter construction. Specifically, it is important that guard rings be installed around all anode outputs. The normal function of guard rings is to reduce the spatial uncertainty and improve the energy resolution of the PSPC by suppressing the anode-to-cathode leakage current, but guard rings also allow bootstrapping of the anode output capacitance to reduce the effective load capacitance and the signal processing time without affecting other parameters.

In most PSPC systems built at ORNL we have used high-input-impedance voltage-sensitive preamplifiers[14,15] to linearly convert the anode signals into low-impedance signals that can be sent over long distances to the signal processing equipment. The high input impedance of these preamplifiers matches the anode RC line impedance well enough to eliminate the need for special termination networks at the PSPC

TABLE I

Available Anode and Cathode Resistance Values and Materials Used in the Experimental PSPCs

Wire Resistivity (Ω/mm)	Material	Diameter (μ)	Source
8000	carbon[a]	25	Zvanut Co.[b]
1500	carbon[a]	75	Zvanut Co.
1000-8000	carbon[c]	25	Zvanut Co.
50-1500	carbon[c]	75	Zvanut Co.
30	Moleculoy	7.3	Molecu-Wire Corp.[d]
18-6	304 SS	7.3-13	California Fine Wire Co.[e]
0.3	Nichrome	75	Sigmund Cohn Corp.[f]

[a]Pyrolytic-carbon-coated quartz fiber.

[b]Carl M. Zvanut Co., 14 Chetwynd Road, Paoli, Pa. 19301.

[c]C. J. Borkowski and J. A. Williams decreased the fiber resistance by resistive self-heating the pyrolytic carbon film in an atmosphere of propylene at 4 cm Hg pressure, thus depositing additional carbon and increasing the pyrolytic carbon film thickness.

[d]Molecu-Wire Corp., P. O. Box 495, Farmingdale, N.J. 07727.

[e]California Fine Wire Co., P. O. Box 446, 338 S. 4th St., Grover City, Ca. 93433.

[f]Sigmund Cohn Corp., Mt. Vernon, N.Y.

outputs in most cases. We recommend that the preamplifier input leads be as short as possible to reduce stray capacitance, because stray capacitance is a load impedance that causes an increase in the signal processing time. It is good practice to mount the high-input-impedance preamplifiers directly on the PSPC cathode.

II. AREA COUNTERS

Several configurations for area (two-dimensional) PSPCs have evolved from the configuration of the linear PSPC (Figure 2). One step in this evolution is to split the cathode of the linear PSPC (Figure 2a) into two halves (Figure 2b) and place several anode wires between the upper and lower cathodes (Figure 2c). Each anode then operates as an independent linear PSPC, where the x-y coordinates of a detected charge Q_{IN} are determined from knowledge of which anode wire and where on this anode wire the charge was deposited. Since each anode is an independent PSPC, this sytem can process high count rates (50,000 counts/s per wire) but requires connection of two preamplifiers per anode.

For most applications the count rates are sufficiently low to permit the simplification indicated in the next configuration (Figure 2d),[4,5] where adjacent anode wires are connected with resistors to form an anode matrix with four outputs. Only four preamplifiers are required to decode the position coordinates of Q_{IN}. Any combination of the configurations illustrated in Figures 2c and 2d can be constructed to optimize the count-rate capability and the simplicity.

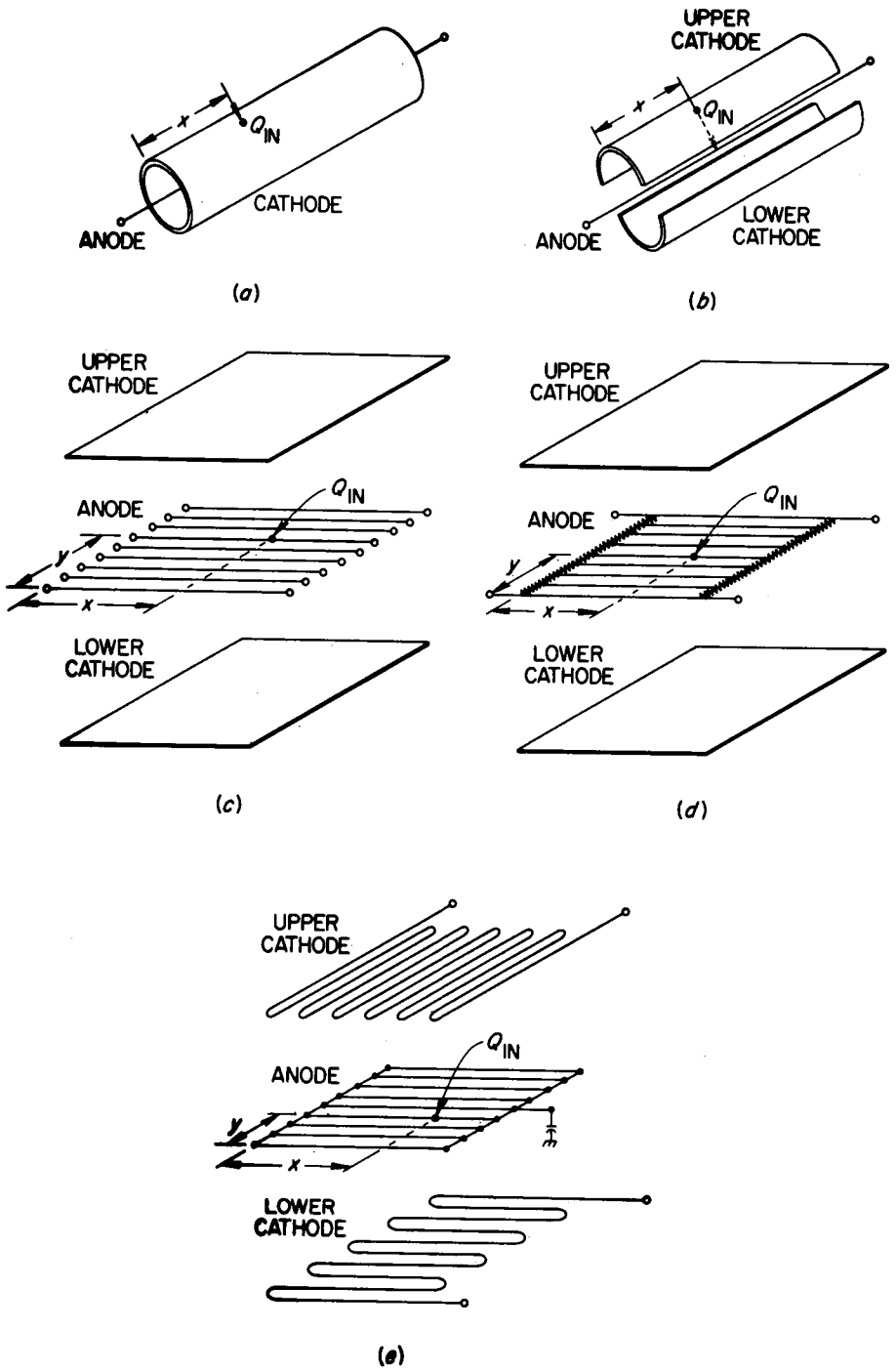


Figure 2. Diagram of the principal steps in the evolution of an area PSPC. (a) Line PSPC, (b) line PSPC with split cathodes, (c) multianode area PSPC, (d) multianode area PSPC with four anode output connections, (e) multianode, all-metal wire area PSPC with grounded anode, two orthogonal cathode RC lines, and continuous wire construction of the anode and cathode planes.

Interconnection of adjacent anode wires with nonzero resistors causes cross modulation between the x and y coordinate signals, such that the image of a square object is distorted to appear as a pincushion. The magnitude of this distortion is proportional to the ratio of the interconnecting resistance to the anode resistance. The values of the interconnecting resistors have to be at least 200 times less than the anode resistance to limit the distortion to < 5% of the anode wire length.

The construction of the anode matrix requires consideration of mechanical details because two low-resistance connections must be made to each anode wire and all interconnecting resistors require mechanical supports. Thus, outgassing materials which must be included in the counter gas volume can seriously degrade the performance of the PSPC.

The spatial resolution along the anode wires remains that of an independent linear PSPC for a matrix of up to 30 wires. We have reported 24,000 resolution elements for a 30-wire, area PSPC with 120-mm-long anodes;[4,5] this is equivalent to a spatial uncertainty of 0.15-mm fwhm along any of the anodes.

This configuration (Figure 2d) is useful whenever (1) the spatial uncertainty along the anode wires has to be small, but the spatial uncertainty in the direction across the anode wires is of secondary importance, or (2) the proportions of the counting area are beyond the collection capability of a single-anode PSPC.[4] A typical application of this configuration is the measurement of angular distributions of charged particles in the focal plane of magnetic spectrographs. In

this application the spacing between upper and lower cathodes must be small ($\sim$ 3 mm) to avoid degradation of the spatial resolution caused by the incidence angle of the charged particles. The small spacing limits the collection capacity of a single anode to an $\sim$ 10 mm wide area.[4] Since the beam width at the focal plane is generally greater than 10 mm, several anodes are required to intercept the total beam width. With these anodes connected as in Figure 2d, page 8, each anode can be calibrated individually, such that small variations in resistivity do not affect the overall spatial resolution.

The next configuration (Figure 2e) simplifies the construction, eliminates the (pincushion) distortion, and increases the count-rate capability, but the spatial uncertainty along the anode wires is increased.[6,7] The anode wires operate, as before, as independent proportional counters; however, in this case, all anodes are connected to signal ground potential. Thus, the input charge Q_{IN} does not produce an output voltage pulse on the anode; instead, it causes currents to flow in the cathode circuits. From the relative shapes of these current pulses in each of the two cathodes, the x-y coordinates of the location of Q_{IN} are decoded. The cathodes perform as two independent orthogonal RC lines. The signals from each cathode are electrostatically shielded from the other cathode by the anode grid. The two signals from each cathode are processed as in a linear PSPC. As illustrated in Figure 2e, page 8, the output signals from the upper cathode determine the x coordinate of Q_{IN}, and the output signals from the lower cathode determine the y coordinate of Q_{IN}.

The main advantages of the area counter configuration of Figure 2e, page 8, are as follows. Support of the anode and cathode wire planes by three independent metal frames (aluminum or stainless steel) greatly simplifies the construction of the counter. All three wire grids are metal wires, continuously strung over pretensioned, individual springs. Only a small amount of insulating materials is used so that outgassing and the frequency of counter gas purifications are lessened. (The only outgassing materials are epoxy that supports the cathode wires on their springs without making electrical contact and mica plates that insulate the anode springs from the anode frame. The anode wires are soft soldered to the anode springs.)

The object-to-image transfer of this PSPC configuration is almost linear, and there is negligible edge distortion.[6] The RC lines of both cathodes have low impedance in the frequency range of interest for position decoding because, for a 200- by 200-mm area PSPC, the cathode resistivity is $\sim$60 Ω/wire and the capacitance is $\sim$0.5 pF/wire. With this low impedance the time required to process each position is < 1 μs, and the PSPC can operate at count rates of 50,000 counts/s.

Owing to the low cathode capacitance, the signal-to-noise ratio for 20-keV photons is > 500 at bias levels below breakdown and with moderate gas-multiplication factors well within the proportional region. Consequently, the energy resolution of this low capacitance PSPC is comparable to conventional, multiwire proportional counters of similar size.

Operation of this PSPC configuration depends on close electrical coupling between the anode and cathodes. The optimum distance between wire planes for a 200- by 200-mm area PSPC is $\sim$3 mm. In many cases this short distance severely limits the stopping power of the gas for photons and reduces the detection efficiency of the PSPC. We increased the detection efficiency for this configuration in a photon camera[6,7] by developing and applying linear or spherical electron drift fields.

CHAPTER III

ENERGY LOSS, DETECTION TIME, AND POSITION OF A SINGLE IONIZING EVENT

A portion of the PSPC gas is ionized during the detection process of an arbitrary event (particle or radiation). The number of electron-ion pairs generated is proportional to the energy loss of the ionizing event.[13] The electric fields inside the PSPC cause electrons to drift toward the anode and ions to drift toward the cathodes. The high field intensity proximate to the anode increases the kinetic energy of the drifting electrons until avalanche multiplication occurs. The avalanche multiplication factor is constant; therefore, the total number of electron-ion pairs generated remains proportional to the energy loss of the ionizing event. The avalanche electrons drift toward the anode, and the ions drift toward the cathodes.

The movement of charges in the space between the anode and cathodes causes a current flow in the external circuits that connect the anode and cathodes. The total current that flows between the anode and cathodes is proportional to the number of electron-ion pairs generated and, therefore, a measure of the energy loss of the ionizing event. The energy loss is

$$W \propto nq = \sum_{i=1}^{m} \int_{0}^{\infty} i_i(t)\, dt \qquad (1)$$

where n is the total number of electron-ion pairs generated, q is the charge of an electron, m is the number of circuits that connect the anode and cathodes, and $i_i(t)$ is the instantaneous current in the $\underline{i}$th circuit. The energy loss W is measured by adding the currents from all external circuits that connect the anode and cathodes, but the reference potentials selected or the method of adding do not affect this measurement. Determination of which electrodes of the PSPC should be at ground potential or what impedances should connect the anode and cathode terminals must be based only on signal-to-noise ratio considerations for the PSPC output signals.

We define the detection time (t_d) of the event as the time of interaction between the event and the PSPC gas. The value of t_d is estimated from the measurement of the shape of the energy-loss signal.

The uncertainty in the estimate of the energy loss and the detection time as a function of the event position is discussed in Chapter VI. All other sources of uncertainty in the energy-loss and detection-time estimates are the same as in conventional proportional counters. They have been covered extensively in the literature[13] and, therefore, are not discussed in this thesis.

We define the position of the detected event as the position of the point source from which the event originated. To relate this event position to the anode of a linear PSPC, we define a Cartesian coordinate system such that its x axis is coincident with the anode wire (Figure 3a). Then, for this linear PSPC, we define the position of a point anywhere on a plane x = a as the point $P_1(a,0,0)$ which is located

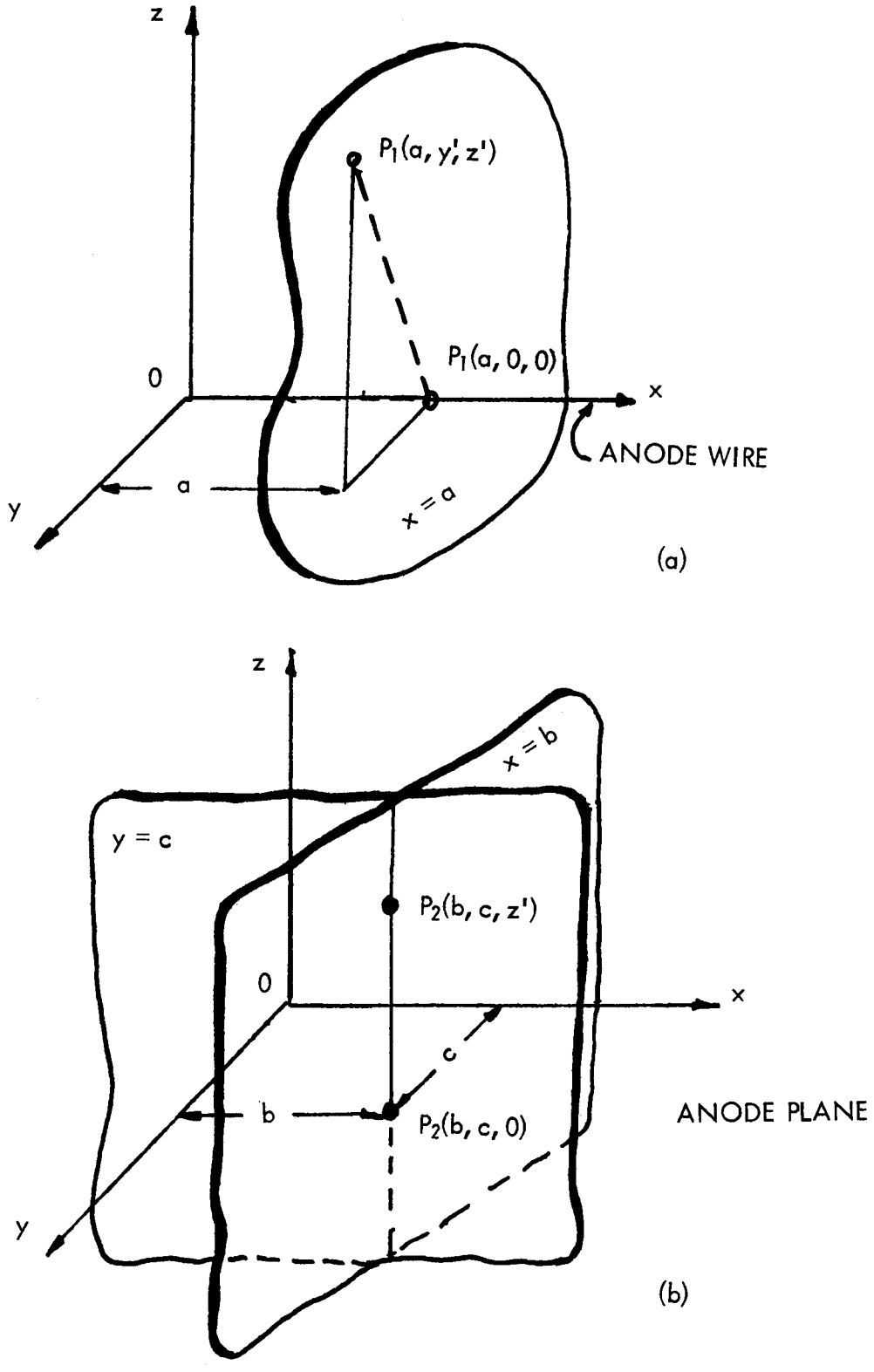


Figure 3. Relation between the source position and the anode of (a) a line PSPC and (b) an area PSPC.

on the anode wire. For an area PSPC, the coordinate system is defined such that its z = 0 plane is coincident with the PSPC anode plane, (Figure 3b). Then, for this area PSPC, we define the position of a point anywhere on the line of intersection of the planes x = b and y = c as the point $P_2(b,c,0)$ which is located in the anode plane.

The position of an event is estimated from the measurement of the output signals from the position decoding circuit. This measurement is modulated by a number of uncorrelated sources of spatial uncertainty (discussed in Chapter V). To characterize these sources of spatial uncertainty, we define the following terms: The position coordinates of the point source from which the detected event originates are (x_s, y_s) (referred to the anode plane). The event may interact with the PSPC gas at a position that is different from the source position; we call the coordinates of this interaction point (x_i,y_i). The charge that is generated in the detection process may have a centroid that is not coincident with the interaction point; the coordinates of this charge centroid position are defined as (x_c,y_c). As the primary electrons generated in the detection process drift toward the anode, the charge centroid position may change; therefore, the coordinates of the transmitted position (i.e., the charge centroid of the electrons generated in the avalanche multiplication) generally differ from (x_c,y_c); we call the coordinates of the transmitted position (x_t,y_t). The estimate of the source position from the transmitted position is generally affected by thermal noise; therefore, the estimated position of a single detected event is generally different from the transmitted position; we call the coordinates of the estimated position (x_e,y_e).

For a line PSPC, the coordinates of the source position, interaction point, charge centroid, transmitted position and estimated position are called (x_s), (x_i), (x_c), (x_t), and (x_e), respectively.

CHAPTER IV

SIGNAL PROCESSING FOR A SINGLE IONIZING EVENT

In this section we shall discuss the RC position encoding method for a single ionizing event and derive expressions for the PSPC output signals in terms of PSPC parameters, load impedance, and event position. We shall describe how the position coordinates of the event are decoded by appropriate pulse shaping and consequent time-difference measurement.

In our opinion, the time-difference measurement has several advantages over amplitude measurement. For example, with a timing system composed of commercial units, we resolve 10^3 spatial elements with negligible long-term drift; the timing uncertainty is generally $< 2 \times 10^{-10}$s rms, and our experience indicates that circuit adjustments for timing are generally simpler and less critical than for amplitude measurements.

I. RC-ENCODING OF POSITION, ENERGY LOSS, AND DETECTION TIME

The output terminals of the area PSPC are interconnected such that the x-coordinate signals are independent of the y-coordinate signals.[4,6] Owing to this signal separation, discussion of RC position encoding in any area PSPC can be reduced to a discussion of two independent, orthogonal, linear PSPCs.

The output signals of such a linear PSPC in response to a detected ionizing event at the position $x = x_e = x_s$ are modulated by the load

impedance Z_L interacting with the portion of the anode-cathode network that is connected between x and each output terminal. Generally, this anode-cathode network can be considered a distributed RC line (Figure 4). The RC line with distributed parameters is described by the following relations.[16]

$$V_g = Z_1 I_g + Z_2 I_0$$

and (2)

$$V_0 = Z_2 I_g + Z_1 I_0$$

where $Z_1 = Z_0 \coth p\ell$, $Z_2 = Z_0 \operatorname{csch} p\ell$, $Z_0 = R_0/p$, and $p = (R_0 C_0 s)^{\frac{1}{2}}$. Further, ℓ is the RC line length, R_0 and C_0 are the distributed resistance and capacitance of the RC line, s is the Laplace transform variable, and I_g and V_g are the Laplace transforms of $i_g(t)$ and $v_g(t)$, that is, input current and voltage to the RC line.

A line PSPC of length L can be represented by two distributed RC lines, one, of length $\ell_1 = x$, connected between the source position x and one of the output terminals, and the other, of length $\ell_2 = L - x$, connected between x and the other output terminal (Figure 5). The transfer impedance of the RC lines [Eq. (2)] are $Z_1' = Z_0 \coth px$ and $Z_2' = Z_0 \operatorname{csch} px$ for the RC line of length x, and $Z_1'' = Z_0 \coth p(L-x)$ and $Z_2'' = Z_0 \operatorname{csch} p(L-x)$ for the RC line of length L - x. Assuming that the current generated in the detection of the event is $I_g(s)$, the output voltage signals for a load impedance $Z_L > 0$ are

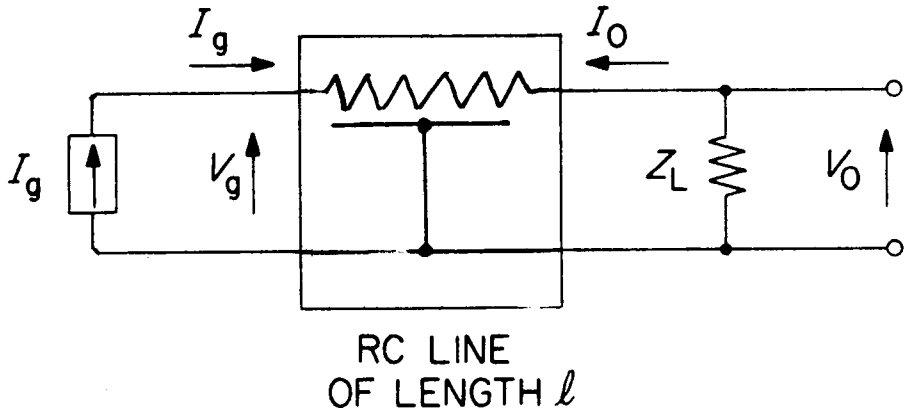


Figure 4. Circuit representation of a distributed RC line of finite length.

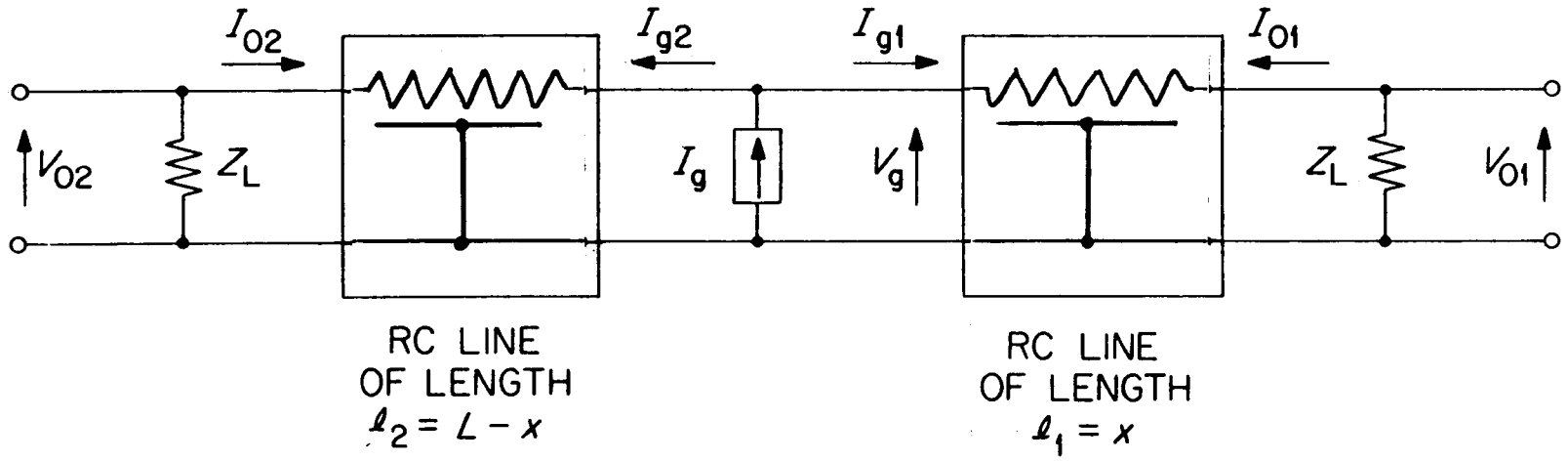


Figure 5. Equivalent circuit of a line PSPC of length L with a current source at the position x.

$$V_{01}(Z_L > 0) = I_g Z_L \frac{\cosh p(L-x) + Z_0 Y_L \sinh p(L-x)}{2\cosh pL + (Z_0 Y_L + Z_L Y_0)\sinh pL}$$

and (3)

$$V_{02}(Z_L > 0) = I_g Z_L \frac{\cosh px + Z_0 Y_L \sinh px}{2\cosh pL + (Z_0 Y_L + Z_L Y_0)\sinh pL}$$

where L is the total length of the RC line, $Y_0 = 1/Z_0$, and $Y_L = 1/Z_L$. The sum of the two output voltages of Eq. (3) is

$$V_{s1}(s,x) = I_g Z_a \cosh p(L/2 - x) \tag{4}$$

where Z_a is a position-independent function of s, R_0, C_0, L, and Z_L. The PSPC output currents for $Z_L > 0$ are

$$I_{01}(Z_L > 0) = -V_{01}(Z_L > 0)/Z_L$$

and

$$I_{02}(Z_L > 0) = -V_{02}(Z_L > 0)/Z_L . \tag{5}$$

The sum of the two output currents of Eq. (5) is

$$V_{s2}(s,x) = I_g Z_b \cosh p(L/2 - x) \tag{6}$$

where Z_b is a position-independent function of s, R_0, C_0, L, and Z_L.

From the relations of Figure 5, the PSPC output currents for $Z_L = 0$ are

$$I_{01}(Z_L = 0) = -I_g \frac{\sinh p(L - x)}{\sinh pL}$$

and (7)

$$I_{02}(Z_L = 0) = -I_g \frac{\sinh px}{\sinh pL} .$$

The sum of the two output currents of Eq. (7) is

$$V_{s3}(s,x) = I_g Z_c \cosh p(L/2 - x) \tag{8}$$

where Z_c is a position-independent function of s, R_0, C_0, L, and Z_L.

In some cases ($L \to 0$, or $Z_L << Z_0$), the distributed capacitance of the PSPC can be neglected. When this is done, the PSPC output voltages are

$$V_{01}(C_0 = 0) = I_g Z_L \frac{R_0(L - x) + Z_L}{R_0 L + 2Z_L}$$

and (9)

$$V_{02}(C_0 = 0) = I_g Z_L \frac{R_0 x + Z_L}{R_0 L + 2Z_L} .$$

The sum of the two output voltages of Eq. (9) is

$$V_{s4}(C_0 = 0) = I_g Z_L . \tag{10}$$

II. POSITION DECODING

For any given line PSPC, the two output signals are processed by identical filters, as shown for the case of the distributed RC line

with $Z_L > 0$ in Figure 6. These filters shape the PSPC output signals into bipolar signals V_{x1} and V_{x2}, where V_{x1} is the filter response to V_{01} or I_{01}, and V_{x2} is the filter response to V_{02} or I_{02}. A desirable pulse shape for crossover timing on the signals V_{x1} and V_{x2} is the derivative of a gaussian or normal density function of time. This function can be sufficiently approximated with commercial nuclear filter amplifiers or with Nowlin's passive filter network,[17,18] with similar results from all. When charge-sensitive preamplifiers are used, the PSPC output signals are step-like functions; therefore, we use the filters in the bipolar mode, because in this mode the step response of the filter yields a bipolar signal that is approximately the desired pulse shape. For current-sensitive preamplifiers, the PSPC output signals are impulse-like functions; therefore, the same filters are used in the unipolar mode, because in this mode the impulse response of the filters yields the desired bipolar pulse shape.

The two filter modes differ in that two RC high-pass filters are used for the bipolar mode, whereas only one RC high-pass filter is used in the unipolar mode. In both modes these filters are band-pass filters with a centerfrequency ω_0.

The filter output signals are processed by the time analyzer to produce the position dependent time interval Δt_c. The logic circuit makes a programmed decision whether to reject or accept any individual signal. In the case of acceptance by the logic circuit, the time interval Δt_c is transformed into a digital signal for computer analysis or multichannel storage or into an analog signal for live display or

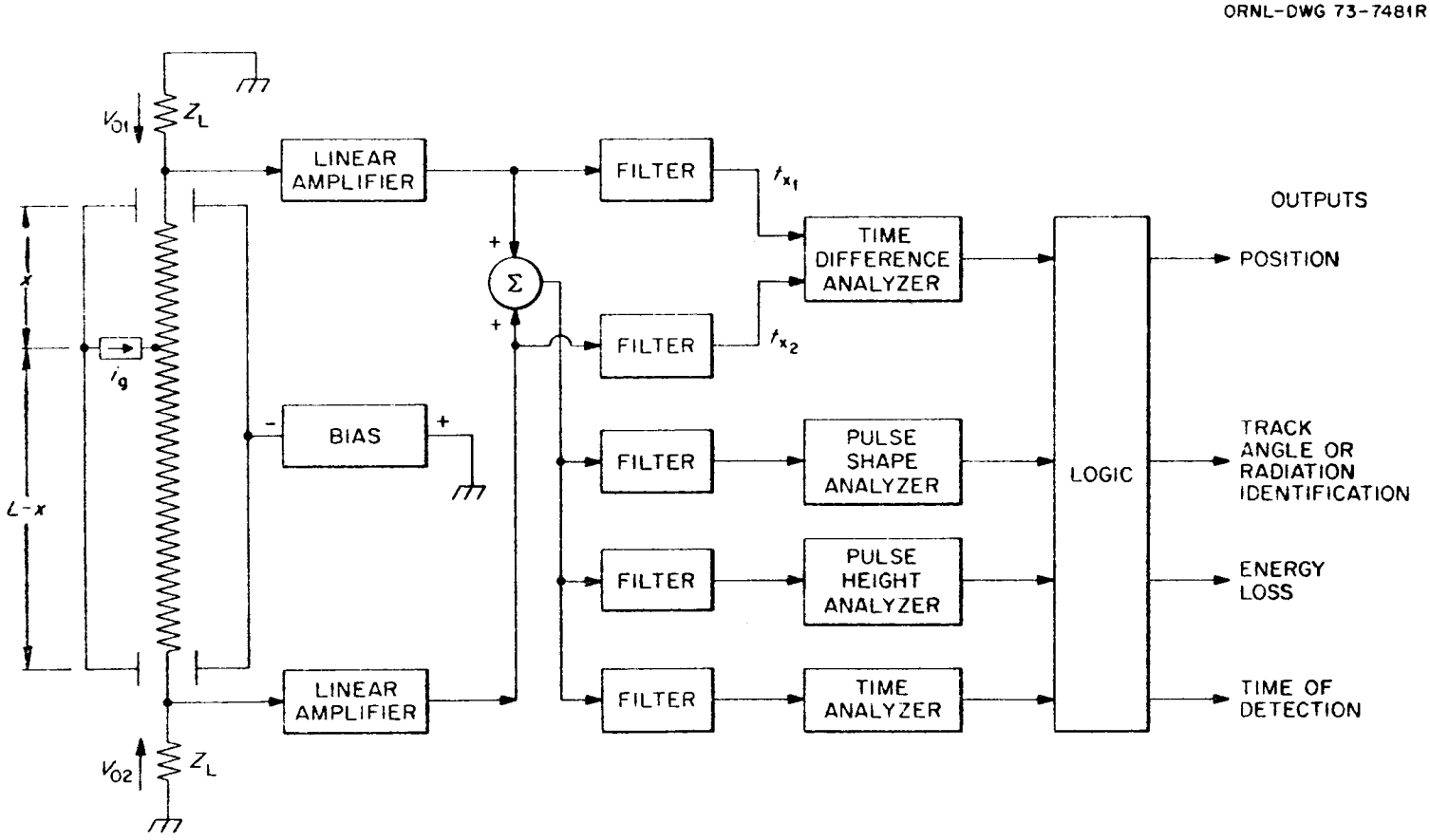


Figure 6. Signal processing circuit for a typical linear PSPC.

storage by a cathode-ray tube. The transfer characteristic of this portion of the signal processing circuit depends on the specific application of each PSPC. Therefore, we shall calculate the position $x = x_e$ from the measured value of Δt_c which is a representative decoder output for the RC position encoding method.

We measure Δt_c at the time analyzer output as the time interval between the zero crossing times of the bipolar signals V_{x1} and V_{x2} such that

$$\Delta t_c = t_{c2} - t_{c1} \tag{11}$$

where t_{c1} and t_{c2} are the zero crossing times of V_{x1} and V_{x2}, respectively. The event position x will be calculated for the most commonly used load impedances: a purely capacitive load, the characteristic impedance of the RC line, and a short circuit.

The bipolar signals $V_{x1}(s)$ and $V_{x2}(s)$ are calculated by multiplying Eq. (3), (5), (7), or (9) by the Laplace transform of the impulse response of the position filter. The resulting event position for any of the three load impedances is of the form

$$x \simeq x_0 + \Delta t_c/S \tag{12}$$

where x_0 is a reference position, and $S = d(\Delta t_c)/dx$ defines the time-to-position conversion factor, or spatial sensitivity.

For the capacitive load or the short circuit, the calculus of the crossover times t_{c1} and t_{c2} is greatly simplified by applying Elmore's definition of delay time.[19] Even though the requirement of monotonic

filter response is violated, this definition yields sufficiently accurate results for estimating the design parameters of most PSPCs. For the capacitive load ($Y_L = sC_L$), no matter whether the output voltage [Eq. (3)] or the output current [Eq. (5)] is measured, and no matter whether the detector is a distributed RC line [Eqs. (3) or (5)] or a lumped RC network [Eq. (9)], we calculate the spatial sensitivity as follows: Assume that the filter impulse response is $H(s) = (1 + h_1 s + h_2 s^2 + \ldots + h_k s^k)/(1 + g_1 s + g_2 s^2 + \ldots\ldots + g_j s^j)$, where h_i, g_i, k, and j are position independent coefficients of the position decoding filter; consider I_g [Eq. (3)] an impulse; replace $Y_L = 1/Z_L = sC_L$ into Eq. (3); and expand the hyperbolic functions of Eq. 3 into power series of the Laplace variable (s). Thus, we have

$$V_{x1} = I_g \frac{(1 + h_1 s + h_2 s^2 + \ldots + h_k s^k)(1 + p_1 s + p_2 s^2 + \ldots.)}{(1 + g_1 s + g_2 s^2 + \ldots + g_j s^j)(1 + q_1 s + q_2 s^2 + \ldots.)}$$

$$V_{x2} = I_g \frac{(1 + h_1 s + h_2 s^2 + \ldots + h_k s^k)(1 + r_1 s + r_2 s^2 + \ldots.)}{(1 + g_1 s + g_2 s^2 + \ldots + g_j s^j)(1 + q_1 s + q_2 s^2 + \ldots.)}$$

where $p_1 = \frac{1}{2} R_0 C_0 (L - x)^2 + C_L R_0 (L - x)$, and $r_1 = \frac{1}{2} R_0 C_0 x^2 + C_L R_0 x$.

Applying Elmore's definition of delay time, and considering that this delay time is the crossover time (t_{c1} or t_{c2}) of V_{x1} or V_{x2}, we have

$$t_{c1} \simeq (h_1 + p_1) - (q_1 + g_1)$$

$$t_{c2} \simeq (h_1 + r_1) - (q_1 + g_1) .$$

Therefore, we have

$$\Delta t_c = t_{c2} - t_{c1} \simeq p_1 - r_1 = \frac{1}{2}R_T C_{GT} + R_0 C_{GT} x ,$$

where $C_{GT} = C_T + 2C_L$, $C_T = C_0 L$, and $R_T = R_0 L$; thus, the spatial sensitivity is

$$S_1(Y_L = sC_L) \simeq R_0 C_{GT} . \tag{13}$$

For the short circuit case (i.e., $Z_L = 0$), we calculate the spatial sensitivity in a similar manner starting with Eq. (7). In this case, the spatial sensitivity is

$$S_1(Z_L = 0) \simeq (1/3)R_0 C_T . \tag{14}$$

For the case where the PSPC load impedance is the characteristic RC line impedance ($Z_L = Z_0$), Elmore's definition of delay time cannot be applied to calculate t_{c1} and t_{c2}, because the expressions for V_{x1} and V_{x2} contain terms with fractional powers of $\underline{s}$ which preclude V_{x1} and V_{x2} from being expressed in the "normalized" form.[19] Therefore, we found an empirical expression for the spatial sensitivity which has a value

$$S_2(Z_L = Z_0) \simeq 2(R_0 C_0/\omega_0)^{\frac{1}{2}} . \tag{15}$$

In practice, for a long PSPC with capacitive load ($C_0 \neq 0$, and $Y_L = sC_L$), we observed that the expression for S_1 [Eq. (13)] is valid only for event positions near the output terminals of the PSPC ($x \simeq L$ or $x \simeq 0$). As the event position approaches the center of such a long

PSPC($x \simeq L/2$), the effect of the load on spatial sensitivity decreases and the value of the spatial sensitivity approaches S_2 [Eq. (15)] as measured for the terminated RC line ($Z_L = Z_0$). We also observed that the spatial sensitivity for capacitive loads can be made practically independent of event position by adjusting the values of C_L and ω_0 such that $S = S_1 = S_2$ anywhere in the PSPC. With this adjustment, solving Eqs. (13) and (15), we have

$$\omega_0(Y_L = sC_L) \simeq 4C_0/(R_0 C_{GT}^2) . \tag{16}$$

For a long PSPC with short circuit load ($C_0 \neq 0$, and $Z_L = 0$), we observed that the expression for S_1 [Eq. (14)] is inaccurate for event positions near the PSPC output terminals ($x \simeq L$ or $x \simeq 0$) where the spatial sensitivity becomes a function ω_0. We also observed that the spatial sensitivity for short circuit loads can be made almost independent of event position by selecting the value of ω_0 such that

$$\omega_0(Z_L = 0) \simeq 4/(R_T C_T) . \tag{17}$$

With this selection, the spatial sensitivity is $S = S_1(Z_L = 0)$ anywhere in the PSPC.

The selection of ω_0 [Eq. (16) or (17)] has several advantages: (1) the PSPC can be linearized without special termination networks; (2) the PSPC can also be linearized for high impedance RC lines where the impedance of the stray capacitance of the PSPC output terminals is usually lower than the characteristic RC line impedance Z_0, which

makes the line termination difficult; and (3) the spatial sensitivity can be adjusted over a wide range for given values of R_0, C_0, and L by selecting appropriate values of C_L and ω_0.

III. ENERGY-LOSS DECODING

As mentioned in Chapter III, we measure the energy loss of a detected event by adding the currents of all external circuits that connect the anode and the cathodes of the PSPC. To make the energy-loss measurement in finite time, the energy-loss information is decoded from the PSPC sum signals V_{s1}, V_{s2}, V_{s3}, or V_{s4} [Eq. (4), (6), (8), or (10)] by band-pass filters that transform the sum signals into unipolar signals of the form

$$V_e(s,x) = F(s) \cosh p(L/2 - x) \tag{18}$$

where $F(s) = (1 + a_1 s + a_2 s^2 + \ldots + a_n s^n)/(1 + b_1 s + b_2 s^2 + \ldots + b_m s^m)$ is position independent, and the coefficients a_i, b_i, n, and m are functions of the PSPC parameters, the load impedance, and the characteristics of the decoding filter.

Since the required decoding filters are linear networks, similar to those used for position decoding, the energy loss is proportional to the filter output signal amplitude in the time domain at an arbitrary measurement time t_m. Generally, we select $t_m = t_p$, where t_p is the time when the filter output signal $v_e(t,x)$ reaches its peak amplitude.

IV. DETECTION-TIME DECODING

The detection time t_d, that is, the time of interaction between an ionizing event and the PSPC gas, is estimated from a bipolar filter output signal of the form $\dot{v}_e(t,x) = \frac{d}{dt}[v_e(t,x)]$. We express t_d in terms of measurable quantities and PSPC properties as

$$t_d = t_e - t_l - t_p \tag{19}$$

where t_e is the best estimate of the zero-crossing time of $\dot{v}_e(t,x)$, i.e., $\dot{v}_e(t_p,x) = 0$; t_l is the electron drift time; and t_e is a position-dependent delay time, defined by the filter properties and the PSPC characteristics.

V. DESCRIPTION OF THE SIGNAL PROCESSING CIRCUIT

The signal processing circuit for a typical line PSPC (Figure 6) operates on the signal described by Eq. (3) to decode and display the information about the position, energy loss, and time of detection of each detected event. All components of this circuit, excepting the preamplifiers, are commercial units.

Each of the two PSPC outputs is connected to a linear amplifier. The input impedance of these amplifiers is represented as part of the load impedances (Z_L) of the PSPC. In most applications, these amplifiers are wide-band, series-feedback amplifiers.[14,15] The input impedance of this amplifier type is approximately capacitive over the frequency band that contains the information to be decoded. With this

approximation the load impedance is $Z_L \simeq (sC_L)^{-1}$, where C_L is the sum of the preamplifier input capacitance and stray capacitance of the PSPC output leads. The value of C_L is $\sim$ 3 pF for most PSPCs. The spatial sensitivity for capacitive load is expressed in Eq. (13).

When shunt-feedback preamplifiers are connected to the PSPC outputs, the condition $Z_L \to 0$ is approached, and the spatial sensitivity is expressed by Eq. (14). Generally, for line PSPCs, the load impedance is $Z_L < Z_0$; therefore, it is not practical to terminate the RC line (equivalent circuit of the PSPC) with its characteristic impedance.

The preamplifiers are designed such that the closed-loop transfer function is almost independent of frequency in the band of interest for information decoding (10 - 10^6 Hz), the gain-bandwidth product is > 350 MHz.[14] The equivalent noise voltage is 1.5 nV/$(\text{Hz})^{\frac{1}{2}}$. The closed-loop voltage gain (A_V) of the preamplifier is matched to the gas multiplication factor of the PSPC and the energy loss of the detected events such that the output pulse amplitudes are $\sim$1 V. Typical values of voltage gain are $5 < A_V < 50$. The preamplifier output impedance is 93 Ω to match the impedance of a coaxial cable and facilitate distortion-free signal transmission over large distances (up to 200 m), whenever the PSPC is remotely operated because of radiation hazards.

The preamplifier outputs are connected to the inputs of a summing amplifier and the position decoding filters. We use a shunt-feedback, wide-band operational amplifier to add the two preamplifier output signals. The summer output signal in response to a detected event has the form of Eq. (18) to decode the energy loss and detection time of the event as for conventional proportional counters.[13]

Both position-decoding filters are identical passband amplifiers that shape the preamplifier output signals into bipolar pulses. The center frequency of the filter passband is selected as specified in Eqs. (16) or (17) to linearize the PSPC (i.e., to make the spatial sensititivty independent of the event position). Generally, it is accepted that a desirable pulse shape for crossover timing is the derivative of a gaussian shaped pulse.[20] We use commercial nuclear amplifiers with active shaping or Nowlin's passive filter amplifier because their response to input step functions is a reasonable approximation to the desired pulse shape. However, we prefer the passive filter amplifier because (1) its step response generates a more symmetric pulse shape than the active filter and, therefore a better approximation to the derivative of the gaussian; (2) the filter can be easily assembled from standard components for any center frequency in a wide range of values (we tested several filters in the range $3 \times 10^4 < \omega_0 < 10^7$ radians/sec), which allows greater flexibility in matching the filter and the PSPC characteristics for linearity as compared to the commercial active-filter amplifiers (generally, only a few switchable center frequencies are provided in the commercial units); and (3) data on noise bandwidth and crossover-time slope are available to calculate the thermal noise in the position signal.[21]

The position-filter outputs are connected to the time-difference analyzer. The output signal amplitude of this unit is proportional to the position of the detected event [Eq. (11)]. Usually, the time-difference analyzer includes the following components: two crossover

detectors, a time-delay generator, and a time-to-amplitude converter (TAC). One of the crossover detectors (CD1) gives an output signal at the zero-crossing time t_{c1} of V_{x1} (Figure 7) and the other crossover detector (CD2) gives an output signal t_{c2} at the zero-crossing time of V_{x2} for each detected event. The delayed signal t_{d1} is the "stop" signal and t_{c2} is the "start" signal for the TAC. Proper operation of the TAC requires the "start" signal always to precede the "stop" signal; therefore, we select a time-delay $DL = t_{d1} - t_{c2} \geq S\Delta x/2$, where $\Delta x (0 \leq \Delta x \leq L)$ is the length of the portion of the PSPC (position window) from which the spatial information is decoded.

Basically, the crossover detectors are Schmitt trigger circuits.[22] The lower level discriminator arms the trigger whenever the input signal exceeds a preset level and its slope is positive. The hysteresis, that is the difference between the upper and lower trigger levels, is such that the trigger resets whenever the input signal passes through a zero level, its slope is negative, and the trigger has been armed previously. The output signal is time-coincident with the trigger reset time t_c.

The basic circuit of the delay generator is a monostable multivibrator.[23] This circuit is triggered by the output signal of the crossover detector and reset after a preselected time interval DL. Thus the output signal of the delay generator occurs at $t_d = t_c + DL$.

The TAC operation is based on a constant current I that charges a capacitor C. The current generator is switched on with the "start" signal and switched off with the "stop" signal. The voltage of the capacitor is $V = (1/C) \int_{start}^{stop} I\, dt = \Delta t I/C$, where Δt is the time

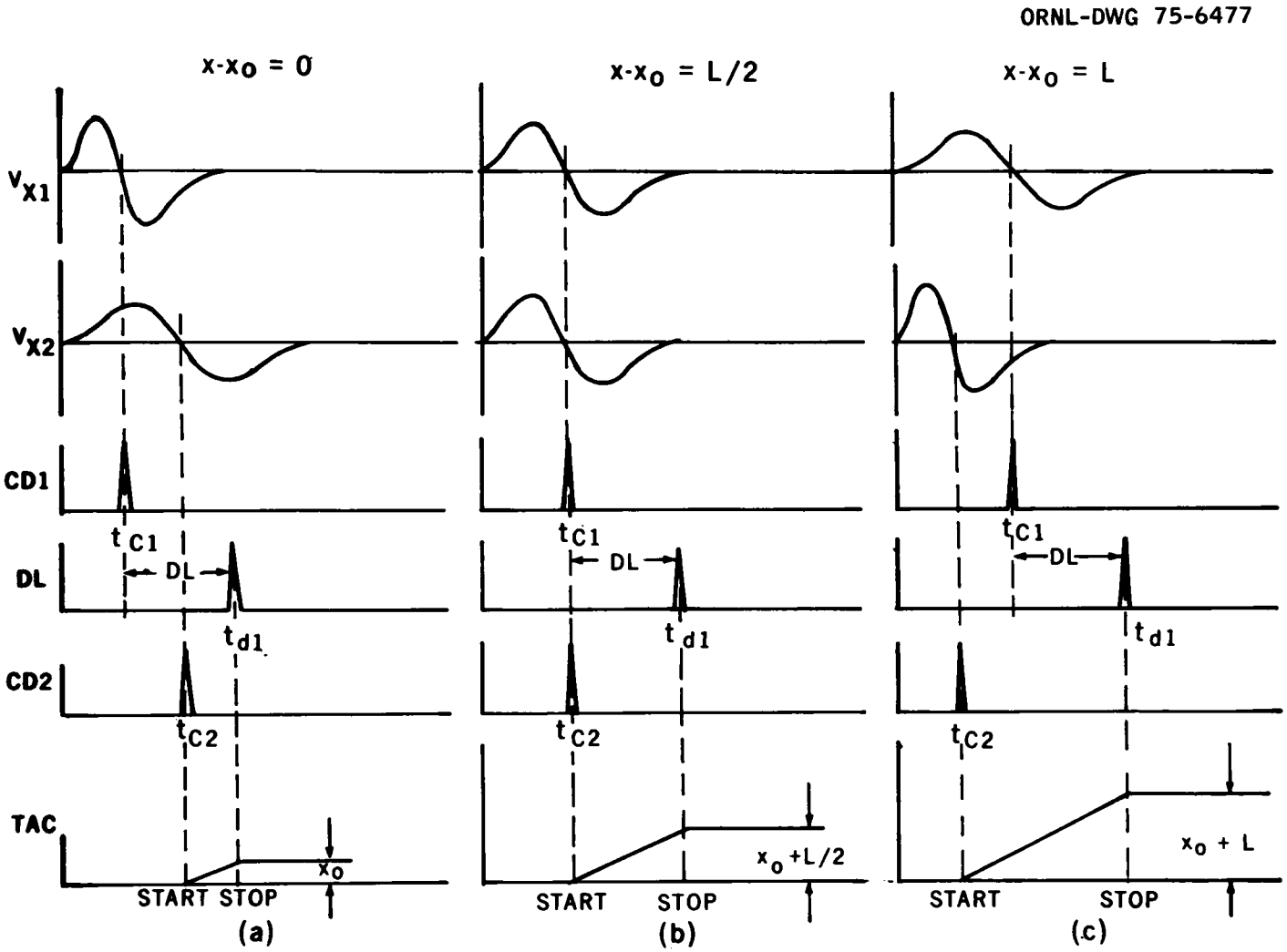


Figure 7. Signal-flow diagram for the time-difference analyzer. The event is detected (a) at the position $x = x_0$, (b) at the position $x = x_0 + L/2$, and (c) at the position $x = x_0 + L$.

interval between the "start" and "stop" signals. Thus, $V = k\Delta t$, where $k = I/C$ is a proportionality constant.

The outputs of the time-difference, pulse-shape, pulse-height, and time analyzers interact in the logic circuit (Figure 6, page 25). The logic is programmed to satisfy specific application requirements of the PSPC and, therefore, cannot be discussed in detail for all applications. Generally, this circuit is composed of logic gates, coincidence circuits, and strobe signals that lock all signals to a reference time for each detected event.

The signal processing time for a typical area PSPC differs from the signal processing circuit of the line PSPC by an additional position decoding circuit for the y-coordinate of the event position. The x- and y-coordinates are decoded independently; the energy loss, pulse-shape and time information is decoded from the sum of the four linear amplifiers, one connected to each output of the two cathodes (Figure 2e, page 8).[6] The decoding of the event coordinates for the area PSPC of Figure 2d is discussed in Reference 4.

CHAPTER V

SOURCES OF SPATIAL UNCERTAINTY

Since the position coordinates x_s and y_s of a detected event are measured independently in an area PSPC, we can simplify this discussion by assuming that the sources of spatial uncertainty in the x-coordinate measurement are not correlated with the sources of spatial uncertainty in the y-coordinate measurement. Therefore, this discussion is limited to spatial uncertainty in a line PSPC. The best estimate x_e of the event position x_s is calculated from the measured time interval Δt_c [Eq. (12)]. If we assume that the uncertainty in Δt_c is proportional to the uncertainty in x_e, i.e., the spatial sensitivity S is a time-invariant calibration constant, the discussion of sources of spatial uncertainty can be limited to the relation between x_s and x_e.

For simplicity, we consider separately the uncorrelated, sequential sources of spatial uncertainty that relate x_e to x_t, x_t to x_c, x_c to x_i, and x_i to x_s. These relations, or probability density functions, are independent factors in the secondary density function that relates x_s and x_e.[21] The relative weights of these factors in determining the total spatial uncertainty are functions of PSPC design parameters and the characteristics of the detected event. Therefore, in most of this section we give only qualitative relations to suggest methods to decrease the spatial uncertainty of the individual probability density functions. The value of the total spatial uncertainty must be estimated individually for each PSPC application.

I. THERMAL NOISE

Thermal noise is the main source of spatial uncertainty in x_e if $x_s = x_t$. The sources of thermal noise are located in the PSPC and in the input circuit of the linear amplifier. In most cases, thermal noise from the PSPC predominates. The amplifier noise has to be considered only in some high count-rate applications and in some area PSPCs.

As an example, we calculate the rms value of the spatial uncertainty caused by thermal noise (P_n) for the following typical conditions: (1) the event position is $x_s = x_t = L/2$, such that in the absence of noise the position filter output signals are $V_x = V_{x1} = V_{x2}$; (2) the PSPC load impedances are capacitive, i.e., $Z_L = (sC_L)^{-1}$; and (3) the values of C_L and ω_0 are adjusted where $S = S_2 = 2(R_0C_0/\omega_0)^{\frac{1}{2}}$[Eqs. (15) and (16)].

The rms value of the spatial uncertainty is $x_n = t_n/S$, where t_n is the rms noise in the position decoder output signal Δt_c [Eq. (11)]. The correlation between the crossover times of V_{x1} and V_{x2} was negligible for all PSPCs that we tested. Therefore, the rms noise in Δt_c can be expressed as $t_n = (2P_n)^{\frac{1}{2}}A_V/S_t$, where A_V is the voltage gain of the position filter and linear amplifier (defined as the peak voltage of V_x in response to a unit step input signal), and S_t the slope of V_x at the crossover time t_c.

For most position filters that we tested, we measured $S_t \simeq A_V V_i \omega_0$, where $V_i \simeq Q/C_{GT}$ is the step-like input voltage that appears at the

amplifier inputs in response to the event detection, and Q the total charge generated in the avalanche ($Q = nq$)[Eq. (1)].

We observed that the power spectral density of P_n is not strongly dependent on frequency in the passband of the position filters and under the conditions of this example. Therefore, we can estimate that the average value of $P_n \simeq 4kTBR_n$ (Reference 24), where k is the Boltzmann constant, $R_n = (R_1^2 + R_2^2)^{\frac{1}{2}}$, R_1 the real part of the complex impedance Z_{in} measured between the anode and cathode terminals of the PSPC at $\omega = \omega_0$, R_2 the equivalent noise resistance of the linear amplifiers, T the absolute temperature of R_n, and B the equivalent noise bandwidth[25] of the position filters, which was measured as $B \simeq \omega_0/2\pi$ for the filters we tested. Consequently, the rms value of the spatial uncertainty caused by thermal noise is

$$x_n \simeq (C_{GT}/Q)(kTR_n/\pi R_0 C_0)^{\frac{1}{2}}. \tag{20}$$

From Figure 5, page 21, we computed $Z_{in} = (Z_0^2 + Z_1 Z_L)/2Z_1 + Z_L + Y_L Z_0^2)$, and using the adjusted value of ω_0[Eq. (16)], we calculated $R_1 = \mathrm{Re}(Z_{in}) \simeq R_T/4$ for all practical values of C_L $(0 < C_L/C_T \leq 1000)$. If we assume $R_1 >> R_2$, the rms value of the relative spatial uncertainty caused by thermal noise is

$$x_n/L \simeq (C_{GT}/Q)(kT/4\pi C_T)^{\frac{1}{2}}. \tag{21}$$

Thus, decreasing the value of C_{GT} reduces the thermal noise in the position decoder, but small values of C_{GT} require high values of ω_0 for

linear operation of the PSPC[Eq. (16)]. However, the upper limit of ω_0 (or the lower limit of C_{GT}) is set by the intrinsic time resolution of the time difference analyzer (Figure 6, page 25). We determined that the rms value of this intrinsic timing uncertainty is usually $<10^{-10}$ rms for commercial filter-amplifiers and crossover timing circuits.

II. DRIFT FIELD DISTORTION

If we assume that $x_s = x_c$ and $x_e = x_t$, the spatial uncertainty is caused mainly by distortions of the electric fields in the electron drift volume of the PSPC; i.e., wherever the equipotential lines of the drift field are not parallel to the anode of the PSPC, the drifting electrons are forced to change their positions with respect to the anode coordinates and, therefore, $x_t \neq x_c$.

For example, the transmitted position x_t in area PSPCs with discrete anode wires is, in most cases, a discrete function in the direction perpendicular to the anode wires in the anode plane. In this direction the equipotential lines near the anode plane focus the drifting electrons. Consequently, with great probability, all primary electrons from any single event produce avalanches entirely on one anode wire, if (1) the dimensions of the primary electron distribution are small compared with the anode wire spacing, and (2) the electron diffusion in the drift region is negligible. Thus, the transmitted position coordinate x_t of such an event is, in most cases, the position of the anode wire nearest to the charge centroid position coordinate x_c. Addition of a drift field to a multiwire area PSPC[6,7] increases the

average diameter of the primary charge distribution because it increases the average drift time during which the primary electron distribution expands by electron diffusion. We observed that the transmitted position x_t approached a continuous function of x_c as the depth of the drift field region was increased, because the average diameter of the charge distribution in each avalanche covered several anode wires. As a result, the spatial uncertainty in a direction across the anode wires was smaller than the wire spacing. However, a further increase in the drift field depth or a decrease in the drift velocity caused the average diameter of the charge distribution to increase to a point where the error in the charge centroid measurement began to control the spatial uncertainty. Therefore, the optimum balance between the detection efficiency and the spatial resolution must be found experimentally for each application by adjusting the drift field depth and the electron drift velocity.

The ions that surround the anode after each avalanche as they drift toward the cathode can cause additional drift field distortions. The number of drifting ions is usually much greater than the number of primary electrons from subsequent events. Thus, the position of drifting electrons from one event is affected by the interaction of these electrons with ions from previous events. Therefore, the spatial uncertainty due to interaction of drifting charges is a function of the number of events detected per unit length of the PSPC in a given time interval and of the time interval during which these charges remain in the PSPC gas.

III. DETECTION PROCESS

The position x_c of the charge centroid of the primary electrons generated in the detection process of an ionizing event is, in most cases, not coincident with the interaction point position x_i. The uncertainty in x_e for $x_s = x_i$ and $x_e = x_c$ depends mainly on the energy loss and the characteristics of the detected event.

Charged Particles

A charged particle in a gas-filled PSPC generally produces an electron-ion track along the trajectory of the particle in the PSPC gas. For a trajectory that is not perpendicular to the anode of the PSPC, the concept of an interaction point is not valid, because the interaction is spread over a space interval Δx_i that has a width $w = d \cos \alpha$, where d is the track length inside the PSPC and α is the track angle with respect to the anode. For such a particle, the charge centroid position x_c is in Δx_i and depends on the specific ionization of the electron-ion track.

Owing to the large number of application possibilities of PSPCs to detect charged particles, a detailed discussion of possible ways to reduce the spatial uncertainty in the detection process of these particles is beyond the limits of this paper. In general, however, we applied the following guidelines to reduce this uncertainty: (1) the depth of the PSPC traversed by a particle was reduced to decrease Δx_i to acceptable values for the smallest possible angle α; (2) the gas pressure was raised to increase the specific ionization along the track;

and (3) the gas multiplication was adjusted to obtain PSPC output signals above the thermal noise level.

Thermal Neutrons

Detection of a thermal neutron in gas mixtures that contain $^{10}BF_3$ or ^3He generates two charged particles at the point of interaction. The two electron-ion tracks of these particles originate at the interaction point and are in opposite directions. Any orientation of this track pair is equally probable. The lengths of the tracks are determined by time-invariant gas and PSPC properties. Therefore, the locus of the charge centroid of the electrons in the track pair is a sphere centered at the interaction point. The diameter of this centroid sphere usually determines the spatial uncertainty in the measurement of thermal neutron positions.

We tested and applied several methods to reduce the spatial uncertainty in the detection process for thermal neutrons. We used $^{10}BF_3$ gas mixtures because the radius of the centroid sphere in this gas is ~ 0.5 the radius of the centroid sphere in ^3He gas at equal pressure; added Xe to the $^{10}BF_3$ gas to further reduce the centroid sphere radius by reducing the track length of the charged particles; measured the track orientation for each detected event; calculated the probabilistic point spread function[21] of each x_i and each orientation; and applied spectrum deconvolution to unfold spatial frequency distributions of detected neutrons from the measured spectra of estimated positions.[26] With the application of these methods, we reduced the spatial uncertainty for thermal neutrons to 0.3 mm fwhm (Figure 8).

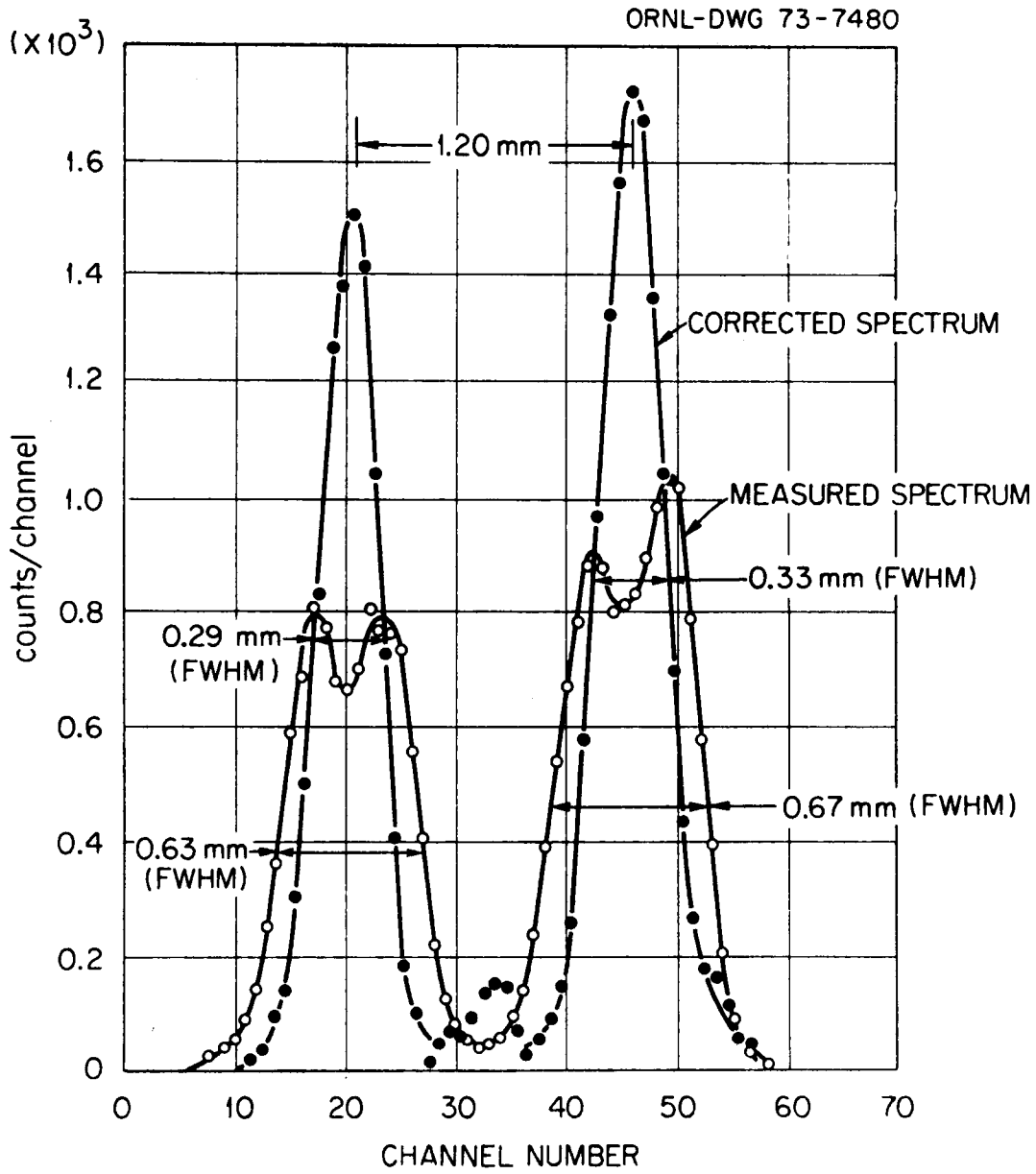


Figure 8. Spatial distribution of thermal neutrons measured with a linear PSPC in response to two, collimated and parallel neutron beams, spaced 1.2 mm, that intercept the PSPC perpendicularly to the anode. The effect of spectrum deconvolution is shown (corrected spectrum).

Low-Energy Photons

The most frequently used counter gas mixtures for the detection of low-energy photons (1-100 keV) contain noble gases. In such gases two energy conversion possibilities exist for a detected photon:
(a) generation of electron-ion pairs near the interaction point, or
(b) generation of a fluorescent x ray and electron-ion pairs near the interaction point. In the first case, the interaction point and the centroid position of the generated charge are almost coincident. In the second case, the fluorescent x ray can escape from the sensitive volume of the PSPC, or it can be reabsorbed at any position in this volume.

When the fluorescent x ray escapes, the remaining energy W_1 of the photon causes ionization around the interaction point x_i. The charge centroid of this distribution is almost coincident with x_i. Thus, the event is recorded at the centroid position $x_c \simeq x_i$, but as having lost an amount of energy $W_1 = W - W_2$, where W is the total photon energy and W_2 the energy of the fluorescent x ray.

When the fluorescent x ray is reabsorbed at a position x_i^1, it ionizes the gas around the new interaction point. For simplicity, we assume that the fluorescent x ray loses all its energy W_2 at x_i^1 and the generation of ions and electrons at x_i and x_i^1 occurs simultaneously. If the two interaction points are equidistant from the anode, the two avalanches occur simultaneously, and the event is recorded as having the position $x_c = (x_i W_1 + x_i^1 W_2)/W$. The recorded energy loss is W. Thus, the position information of the event has been distorted without

affecting the energy information. If the two interaction points are not equidistant from the anode, the two avalanches do not occur simultaneously. In this case, one can attempt to avoid registration of the event by time-coincidence discrimination.

IV. SOURCE POSITION

The relation between x_e and x_s for $x_i = x_e$ depends on the characteristics of the ionizing event and on the collimator that couples the source to the PSPC. Generally, a known relation between the source position and the PSPC coordinates is established first by a collimator or a pinhole that transmits only those events that follow a prescribed path between the source and the PSPC.

When this prescribed path is not perpendicular to the anode and the source emits neutrons or photons, the nonzero thickness of the PSPC is a source of spatial uncertainty. Any of the neutrons or photons can interact with the PSPC gas anywhere along the portion of the path contained inside the PSPC volume. The probability of interaction is greatest at position x_2 where the path enters the PSPC and decreases exponentially toward the exit position x_1 of the path (Figure 9). The shape of the resulting probability density function for the event interacting at $x_1 \leq x_i \leq x_2$ depends on the PSPC depth, the path angle, and the gas absorption coefficient.

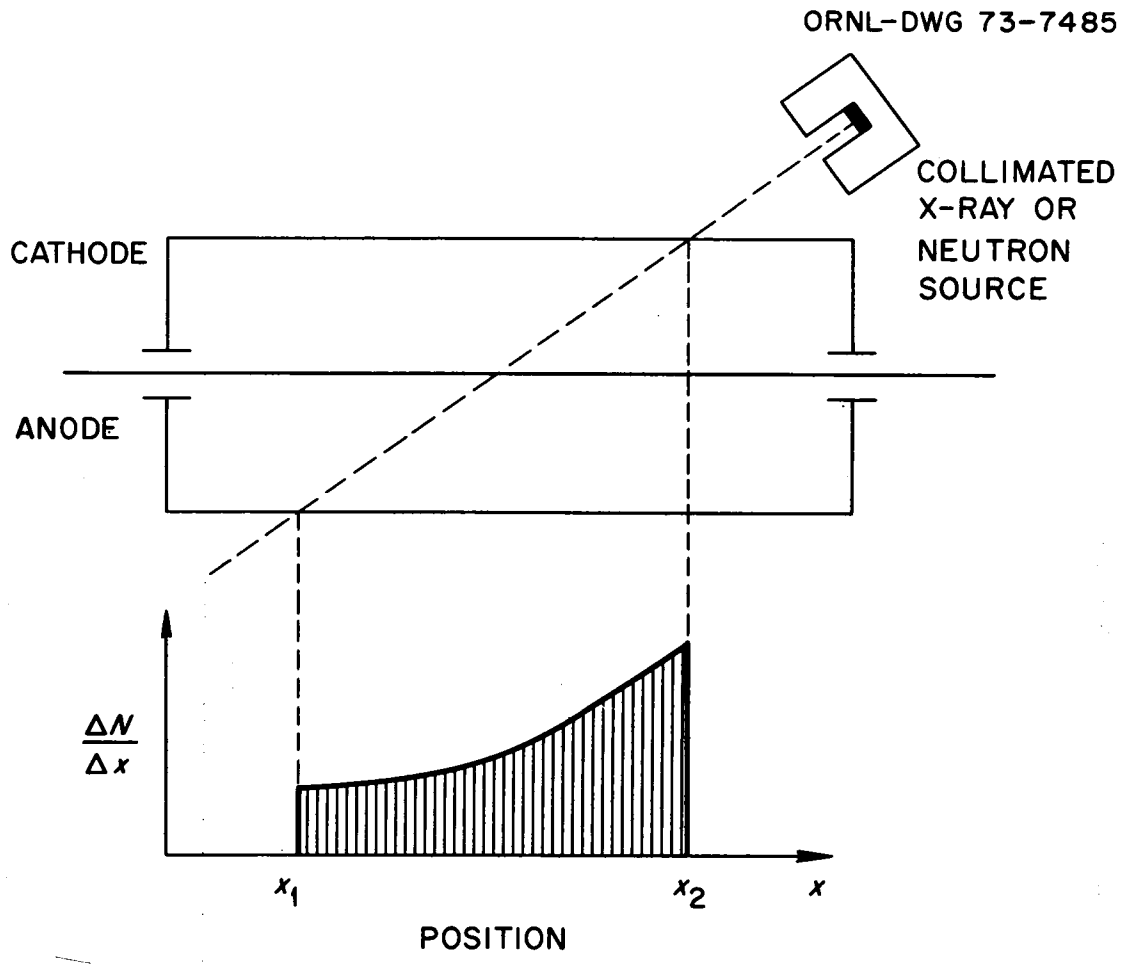


Figure 9. Measurement geometry of a neutron or x-ray source position and the resulting probabilistic point spread function (assuming $x_i = x_e$).

CHAPTER VI

ERRORS IN THE MEASUREMENT OF ENERGY LOSS AND DETECTION TIME

The estimate of energy loss and detection time from Eq. (18) is affected by the event position and by statistical errors similar to those in conventional proportional counters. Thermal noise and avalanche multiplication uncertainty—the main components of the statistical errors—have been extensively discussed in the literature.[13] Therefore, this discussion is limited to the position-dependent error in the measurement of energy loss and detection time in a line PSPC.

The calculus of this position-dependent error is greatly simplified by assuming that in the time domain the filter output signal for the energy-loss estimate $[v_e(t,x)]$ has the shape of a normal density function and the filter output signal for the detection-time estimate is $\dot{v}_e(t,x) = d[v_e(t,x)]/dt$.[27] The errors calculated under this assumption have been verified by measurements on a variety of PSPCs to within experimental errors.

Experimental results also indicate that for a line PSPC of length L ($0 \leq x \leq L$), neglecting statistical errors and assuming an arbitrary energy loss of the detected event, we have

$$0 < v_e(t_{p1},L/2) \leq v_e(t_{px},x_1) \leq v_e(t_{p2},0) = v_e(t_{p3},L) \qquad (22)$$

where t_{p1}, t_{px}, t_{p2}, and t_{p3} are the peak times of $v_e(t,x)$ at the

positions $x = L/2$, x_1, 0, and L, respectively, and x_1 is an arbitrary position in the interval $(0 \leq x_1 \leq L)$.

Thus, we define the maximum position-dependent error in the energy-loss measurement as

$$\varepsilon_e \equiv 1 - v_e(t_{p1}, L/2)/v_e(t_{p2}, 0) \ . \tag{23}$$

Assuming the shape of a normal density function we have

$$v_e(t,x) = (2\pi\sigma)^{-\frac{1}{2}} \exp[-(t - t_p)/(2\sigma)^2] \ . \tag{24}$$

For $x = 0,L$, we have $\sigma = \sigma_2$ and $t_p = t_{p2}$; and for $x = L/2$, we have $\sigma = \sigma_1$ and $t_p = t_{p1}$ (Figure 10a). Applying Elmore's definition of rise-time[19] we have $t_{r1} = (2\pi)^{\frac{1}{2}} \sigma_1$ and $t_{r2} = (2\pi)^{\frac{1}{2}} \sigma_2$; and since $\sigma_2/\sigma_1 = v_e(t_{p1}, L/2)/v_e(t_{p2},0)$, we have

$$\varepsilon_e = 1 - (\sigma_2/\sigma_1)^{\frac{1}{2}} = 1 - (t_{r2}/t_{r1})^{\frac{1}{2}} \ . \tag{25}$$

From Eq. (18) we have for $x = 0, L$

$$V_e(s,0) = V_e(s,L) = F(s) \cosh (pL/2) = F(s) \cosh (Ts)^{\frac{1}{2}} \tag{26}$$

where $T = R_T C_T/4$. Expanding the terms we have

ORNL-DWG 75-6478

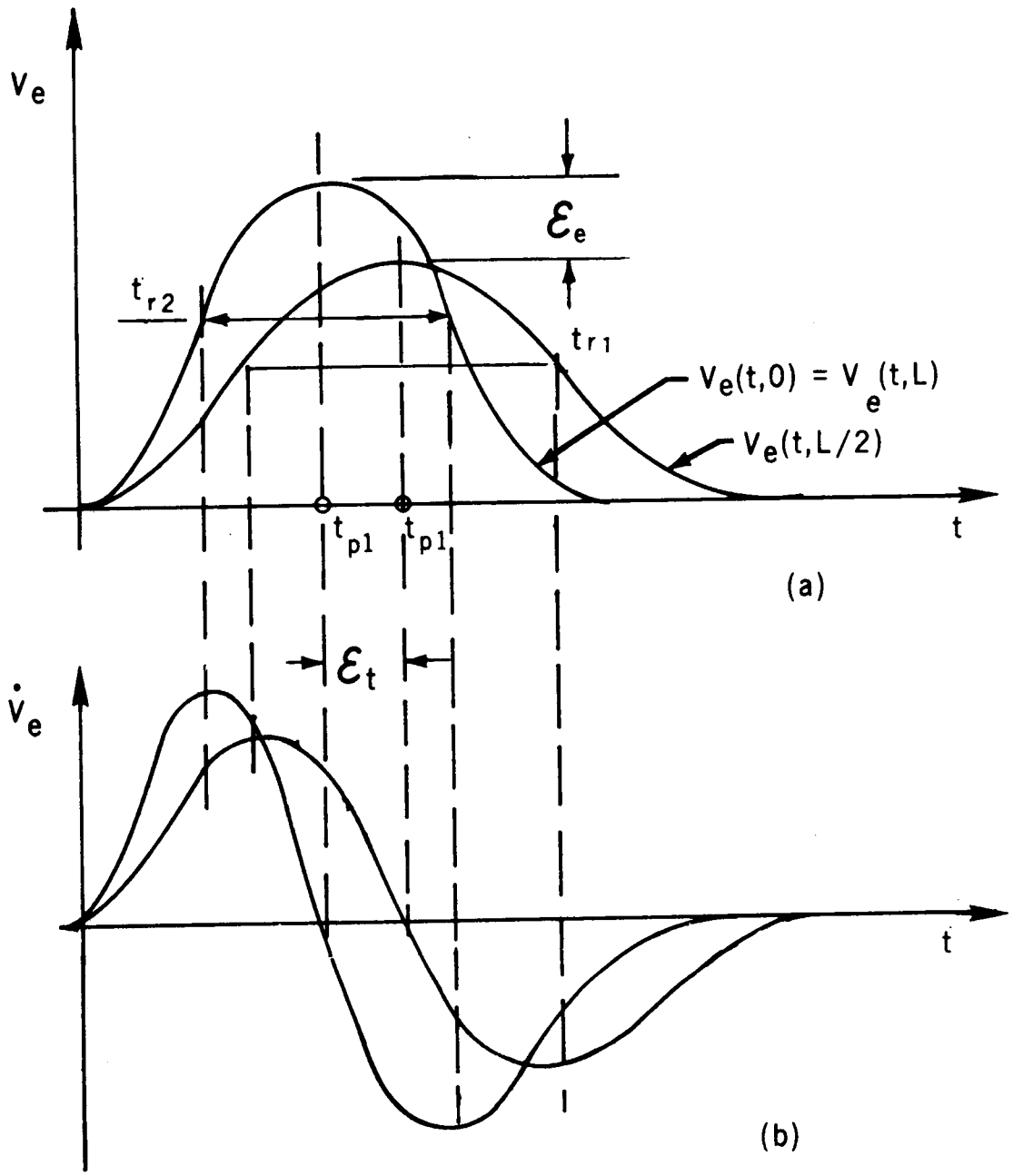


Figure 10. Approximate shapes of the filter output signals (a) for the energy-loss measurement and (b) for the detection-time measurement, represented for two event positions: x = 0 and x = L/2.

$$V_e(s,0) = \frac{1 + a_1 s + a_2 s^2 + \ldots + a_n s^n}{1 + b_1 s + b_2 s^2 + \ldots + b_m s^m} \left[1 + \frac{Ts}{2} + \frac{(Ts)^2}{24} + \ldots\ldots\right]$$

$$= \frac{1 + s(a_1 + T/2) + s^2(a_2 + T^2/24 + a_1 T/2) + \ldots\ldots}{1 + b_1 s + b_2 s^2 - + \ldots\ldots} \qquad (27)$$

Applying Elmore's definition of delay- and rise-time, we have

$$t_D(0) = t_{p2} = b_1 - a_1 - T/2 , \qquad (28)$$

$$t_R^2(0) = t_{r2}^2 = 2\pi(b_1^2 - a_1^2 + 2a_2 - 2b_2 - T^2/8) . \qquad (29)$$

Similarly, from Eq. (18), we have for x = L/2

$$V_e(s,L/2) = F(s) = \frac{1 + a_1 s + a_2 s^2 + \ldots + a_n s^n}{1 + b_1 s + b_2 s^2 + \ldots + b_m s^m} , \qquad (30)$$

and, therefore

$$t_D(L/2) = t_{p1} = b_1 - a_1 , \qquad (31)$$

$$t_R^2(L/2) = t_{r1}^2 = 2\pi(b_1^2 - a_1^2 + 2a_2 - 2b_2) . \qquad (32)$$

From Eqs. (29) and (32) we have

$$t_{r1}^2 = t_{r2}^2 + \pi T^2/4 . \qquad (33)$$

From measurements we determined that the step response of most nuclear filter amplifiers in the "unipolar" mode is an approximation to the

normal density function with a variance $\sigma_1^2 = t_{r1}^2/2\pi \simeq 1/\omega_0^2$. Thus, replacing the values for t_{r1} and T, we have from Eqs. (25) and (33)

$$\varepsilon_e = 1 - [1 + T^2/(8t_{r1}^2)]^{-\frac{1}{4}}$$

$$\simeq 1 - [1 + (0.1R_TC_T\omega_0)^2]^{-\frac{1}{4}} . \qquad (34)$$

We define the maximum position-dependent error in the measurement of the detection time (Figure 10b, page 50) as

$$\varepsilon_t \equiv t_{p1} - t_{p2} . \qquad (35)$$

From Eqs. (28) and (32) we have $t_{p1} = t_{p2} + T/2$; therefore,

$$\varepsilon_t = T/2 = R_TC_T/8 . \qquad (36)$$

CHAPTER VII

MEASUREMENT RESULTS

We built and tested several line and area PSPCs to (1) verify experimentally the relations established in this paper; and (2) apply these relations to reduce the spatial uncertainty, shorten the signal processing time, and increase the count-rate capability of these PSPCs.

I. SPATIAL UNCERTAINTY FOR ALPHA PARTICLES AND X RAYS

A high-resolution, line PSPC was designed for position measurement of alpha particles and x rays. Applying the noise considerations of the previous section, we fabricated a PSPC which we describe as follows. The cathode is cylindrical and 2 mm in diameter. The anode is a 25-μ-diameter, pyrolytic-coated quartz fiber (Table I, page 6) with 8 kΩ/mm resistivity and is mounted coaxially inside the cathode. The active PSPC length is 25 mm. We solved the mounting problem for such a short anode wire and reduced the field distortion by using a total length of quartz fiber of 100 mm and centering it inside an electrostatic shield of 4×10 mm^2 rectangular cross section, with the cathode surrounding the anode wire over 25 mm of the center section of this shield. The total counter resistance R_T was reduced to 200 kΩ by evaporating a gold film on the two, 37.5-mm-long, quartz-fiber sections outside the cathode. The total counter capacitance (C_T) is 0.3 pF. The load capacitances (C_L) total 3 pF: the capacitance between the shield and the gold-covered

position of the quartz fiber is 0.5 pF, the preamplifier input capacitance is 2 pF, and the stray capacitance is 0.5 pF (the guard-ring capacitances are bootstrapped; i.e., they are connected to the sources of the input transistors and do no appreciably increase C_L).

With a selected filter center-frequency (ω_0) of 1.26×10^5 radians/s[Eq. (16)], the spatial sensitivity of this PSPC is independent of position, i.e., S is $\sim$50 ns/mm anywhere along the anode. The equivalent thermal noise resistance (R_n) of this PSPC is $\sim$50 kΩ; therefore, the calculated thermal noise contribution to the spatial uncertainty (x_n) for an input charge of 10^{-12} coulomb is 6 μ rms[Eq. (23)].

We measured the spatial uncertainty for collimated ^{242}Cm alpha particles with this high-resolution PSPC. The bias was set at 900 V to generate a charge of 10^{-12} coulomb for each detected alpha particle. The gain of the time analyzer was 2.08 channels/ns, and the total gain of the position signal filter was 100 channels/mm. A 25-μ-wide slit through the cathode (Figure 11) collimated the alpha particles. Two 0.5-mm-diameter holes, spaced 2.9 mm between centers, were a spatial reference for the position scale calibration. The PSPC was operated with 90% Ar-10% CH_4 at 1 atm flowing through the cathode.

The alpha-particle count rate was 1.5 counts/min through the collimator and 36 counts/min through both reference holes. The spatial resolution test was operated > 20 hr to accumulate 1800 counts in the collimated alpha particle spectrum (Figure 11). The measurement results indicate a spatial uncertainty of 47 μ fwhm (standard deviation of 20 μ). The measured spatial uncertainty was 100 μ at fw(0.1)m and 170 μ at

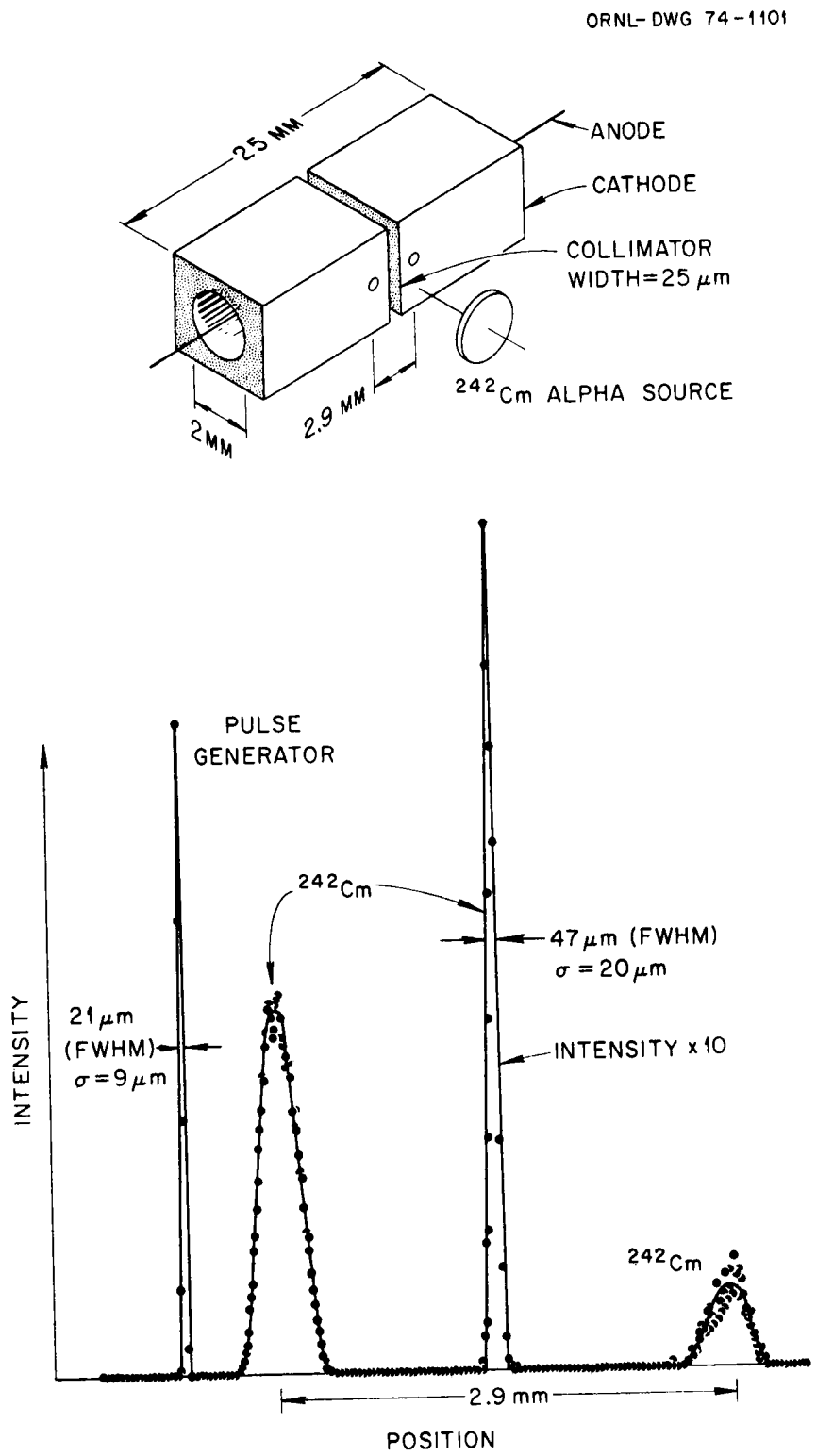


Figure 11. Experimental counter and alpha source measurement geometry showing the measured spatial distribution of alpha particles and the resulting spatial uncertainty.

fw(0.01)m. These uncertainties include thermal noise, long-term drift in the timing channels, and modulation by the finite collimator width.

We estimated the thermal noise plus the long-term drift by measuring the uncertainty in the crossover-time spectrum of a constant-rise-time generated signal that was injected into the position filters $\sim$1 ms after the detection of every alpha particle. The rms uncertainty of this noise spectrum was 9 μ. We estimate that the spatial uncertainty in determining the source position of a ^{242}Cm alpha particle for $x_t = x_e$ is less than 28 μ fwhm.

We measured the spatial uncertainty for low-energy x rays with the same PSPC, gas mixture, and position filters as used for the alpha particle test. However, we increased the bias voltage to 1150 V to increase the gas multiplication for the x-ray detection and generate a total charge of 10^{-12} coulomb in response to the detection of a 3 keV x ray. The x rays were generated in a W-target x-ray tube operating at 10 kV bias. An aluminum collimator between the x-ray tube and PSPC limited the width of the x-ray beam to 25 μ. A two-parameter, multichannel analyzer classified, stored, and displayed the position and the energy loss of the detected x rays. The y-parameter, with eight channels of capacity, was connected to the sum signal and calibrated to display x-ray detection frequency vs energy as follows: $<$ 1.5 keV in channel one, 1.5 to 6.5 keV in 1-keV-wide bands in channels two to seven, and $>$ 6.5 keV in channel eight. The x-parameter, with 512-channels of capacity, was connected to the position signal output. The position signal gain was 100 channels/mm. With this arrangement, six position

spectra were acquired simultaneously, each covering a 1-keV-wide x-ray energy band.

The measurement results (Figure 12) indicate that the spatial uncertainty is $\sim 100\,\mu$ fwhm for 1.5- to 6.5-keV x rays and for a data acquisition rate of 2 counts/s per $25\,\mu$. When the acquisition rate was increased to 20 counts/s per $25\,\mu$, the spatial uncertainty for the same energy band increased to $155\,\mu$ fwhm. In our opinion, this degradation of spatial resolution is not caused in the electronic signal processing circuits, because the total signal processing time is $< 20\,\mu$s/event, and random signals generated at a rate of 5,000 signals/s can be processed without affecting the spatial resolution. Probably, the count-rate-dependent drift-field distortion (Chapter V, II) near the anode caused this increased spatial uncertainty for the low-energy x rays.

The spatial uncertainty in estimating the source position of an x ray for $x_e = x_i$ is probably limited by x-ray scattering in the collimator and in the counter gas.

II. POSITION-SIGNAL PROCESSING TIME

The relation between spatial uncertainty and position-signal processing time was determined by comparison of two line PSPCs. (We define position-signal processing time T_m as the time interval between the detection time and the time at which all filter output voltages have returned to within 5% of their quiescent levels.) Both PSPCs were 500 mm long, were operated with 90% Ar-10% CH_4 at 2 atm, and had 13-mm-diameter cylindrical cathodes. Counter 1 had a 75-μ-diameter

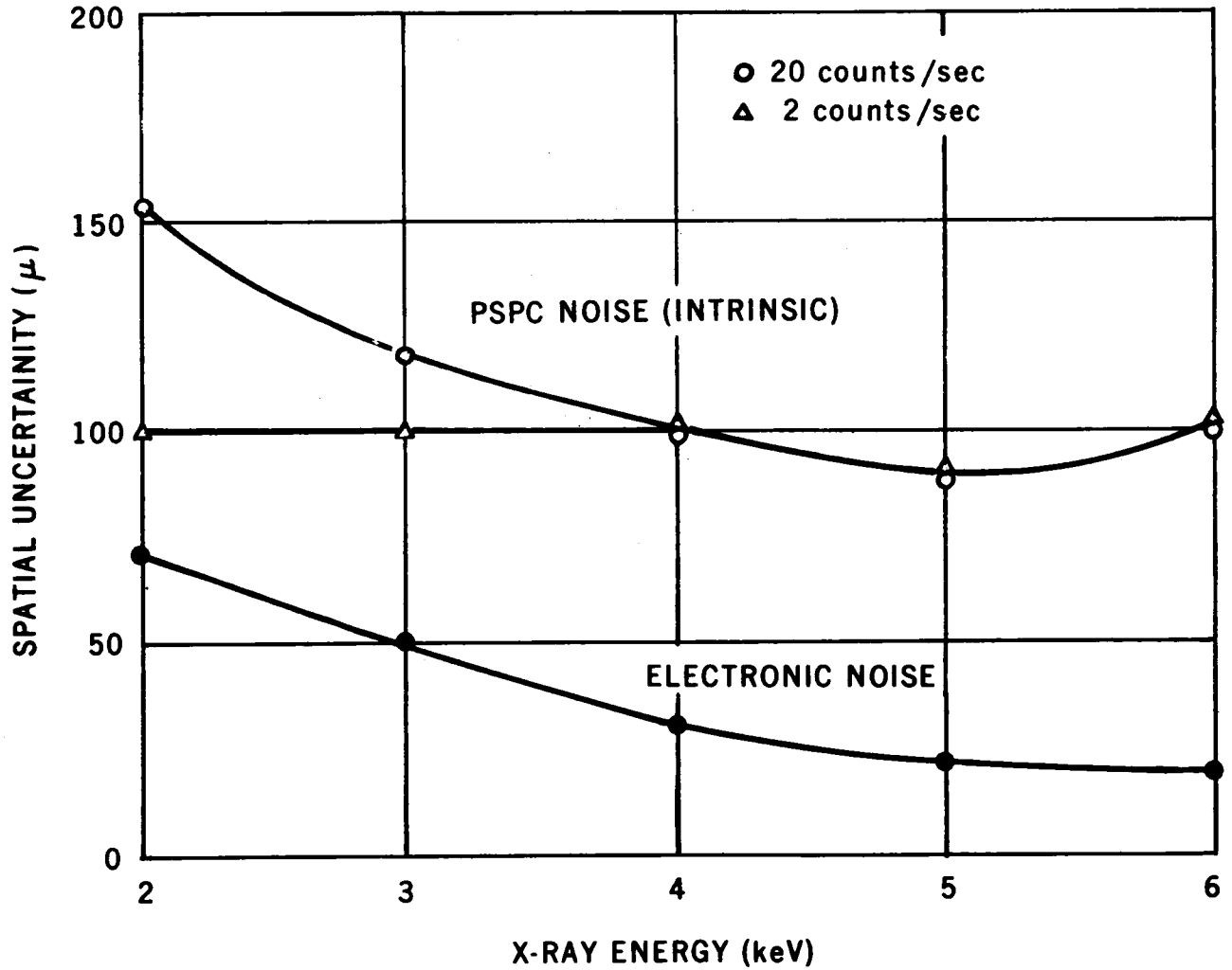


Figure 12. Spatial uncertainty as a function of x-ray energy measured with the PSPC of Figure 11, page 55.

pyrolytic-carbon-coated quartz anode, and counter 2 had a 7.3-μ-diameter stainless steel anode (Table I, page 6).

The center frequencies of the position filter for both counters were adjusted to linearize the spatial sensitivity [Eq. (16)], and the bias voltages were adjusted to generate a charge of $\sim 2 \times 10^{-13}$ coulomb in response to a detected 5.9-keV x ray. The measurement results for the two PSPCs (Table II) show that the value of T_m is 550 ns/event for counter 2, which is 67 times smaller than the value of T_m for counter 1. The main source of spatial uncertainty in both PSPCs is thermal noise, i.e., $x_s \simeq x_t$. The calculated values of x_n[Eq. (23)] are almost equal in both PSPCs. However, the measured spatial uncertainty of counter 2 is four times that of counter 1 because the absolute time resolution of the position filters was limited to $\sim 10^{-10}$ s rms. We used Nowlin's passive filter amplifiers[17,18] in this test.

III. COUNT-RATE CAPABILITY

The effects of high background count rates on spatial uncertainty were illustrated with counter 2 placed in a radiation field of 59-keV gamma rays from ^{241}Am to detect 10^5 gamma rays per second and provide a uniform background over the entire length of the PSPC. Simultaneously, the position of a low-intensity, collimated beam of 5.9-keV x rays was measured. The measured spatial uncertainty without the background was 2.0 mm fwhm (Table II). With the background added, the measured fwhm spatial uncertainty of the 5.9-keV x-ray positions increased to 6.5 mm, while the electronic noise contribution remained ~ 1.8 mm fwhm for both

TABLE II

Results of a Test to Compare the Signal Processing Time and Spatial Uncertainty for Two Linear PSPCs of Similar Design but Having Different Anode Resistances

Variable	Units	Measured or Estimated Values	
		Counter 1	Counter 2
R_o	Ω/mm	1.4×10^{3}	1.8×10^{1}
C_o	F/mm	1.1×10^{-14}	7.5×10^{-15}
ω_o	radians/s	2.0×10^{5}	1.3×10^{7}
C_L	F	3.0×10^{-12}	3.0×10^{-12}
L	mm	5.0×10^{2}	5.0×10^{2}
S	S/mm	1.8×10^{-8}	2.1×10^{-10}
B_m [a]	radians/s	2.2×10^{5}	1.4×10^{7}
R_n [b]	Ω	1.8×10^{5}	1.6×10^{3}
X_n [c]	mm rms	3.9×10^{-3}	4.1×10^{-3}
T_m [d]	s	3.7×10^{-5}	5.5×10^{-7}
x_m [e]	mm rms	2.0×10^{-1}	8.5×10^{-1}

[a] B_m is the measured noise bandwidth of the position filter, i.e., the bandwidth of an ideal, sharp-cutoff filter that has the same rms response to white noise as the position filter.[28]

[b] R_n, the equivalent noise resistance, represents the combined noise that is generated by the PSPC impedance and the position filter [Eq. (23)].

[c] x_n is the rms value of the spatial uncertainty caused by thermal noise [Eq. (23)] calculated for the ratio $C_{GT}/Q = 1$.

[d] T_m is the position signal processing time as defined in the text.

[e] x_m is the measured rms value of the spatial uncertainty for 5.9-keV x rays.

measurements. These results indicate that the spatial uncertainty increases appreciably in high-intensity radiation fields. This poorer resolution was not caused by the RC position encoder or the decoding circuits. More likely, electric field distortions caused by space charge near the anode (Chapter V) were responsible for the increased spatial uncertainty.

CHAPTER VIII

APPLICATIONS

The RC position encoding method was applied to position measurements of low-energy photons, neutrons, and charged particles in a wide variety of nuclear physics experiments; nuclear medicine imaging; and low-dose, medium-resolution radiography.

The linear PSPCs successfully recorded information from focal planes of magnetic spectrographs.[29,30] The authors mention as main advantages for this application the dimensional flexibility, simplicity of operation and calibration, low background count rate per spatial resolution element, and excellent resolution that permits particle identification. Therefore, high precision experiments, such as coulomb excitation, are now possible.

Small-angle x-ray scattering in biomedical samples[31] and magnetic disorder scattering of neutrons in ferromagnetic materials[32] are being studied with linear PSPCs. The area PSPC was applied to study neutron radiography.[33] In these studies the data acquisition times were much less than when other detection systems such as photographic emulsions or scanning detectors were used.

The area PSPC was applied in diagnostic nuclear medicine x-ray imaging of <u>in vivo</u> radioisotope distributions[34] where it is very important to subject the patients to low doses of radiation.

Medium resolution radiographs were produced with a total radiation dose of 10^{-6} roentgen absorbed dose (rad, Reference 6).

Small-angle scattering experiments with low-energy x rays[35] and thermal neutrons[36] are in a final planning stage to determine voids caused by radiation damage in construction materials of liquid-metal fast breeder reactors. In both types of experiments the scattering patterns will be imaged with area PSPCs that use RC position encoding.

An area PSPC (10 by 10 cm) was used in a soft x-ray imaging system for cosmic x-ray studies from rockets.[37] RC position encoding was applied because the wire plane construction with continously strung metal wires (Figure 2e, page 8) is rugged, and the energy resolution for soft x rays is excellent (80% for 250-eV x rays). The PSPC passed without failure the vibration tests required for rocket launching.

CHAPTER IX

CONCLUSIONS

The development of proportional counters with the added capability of encoding the position of individual photons, neutrons, or charged particles without compromising other desirable characteristics such as good energy- and time-resolution has opened several new fields of applications for these position-sensitive proportional counters. Among the most successful applications of these counters are photon imaging of in vivo distributions of radioisotopes in nuclear medicine, low-dose, medium resolution radiography, imaging of x-ray and neutron small angle scattering patterns, and recording of spatial information from the focal planes of magnetic spectrographs.

Position encoding with distributed parameter RC lines is one of the most applied methods because counter construction and signal processing are generally simpler as compared to other position encoding methods. The application of this method has proceeded at a rapid pace even though solid theoretical guidelines and models for this method were not available. Therefore, the main objective of this thesis was to aid in establishing such guidelines, provide approximate models, and verify experimentally their accuracy.

The application of Elmore's definition for rise-time and delay time has greatly simplified the calculus of encoding and decoding parameters for the spatial information. Furthermore, this definition was useful to

linearize the spatial response of the PSPCs, and calculate the errors in the energy loss and timing signals caused by the position encoding.

The spatial sensitivity of PSPCs with RC position encoding was calculated for several load conditions (short circuit, RC-line termination, and capacitive load). It was shown that the position decoding is the same for these three conditions.

A discussion of several sources of spatial uncertainty is presented. It was found that thermal noise in the position signal is almost independent of the magnitude of the distributed resistivity of the RC line, even though this resistance is the main source of thermal noise for most PSPCs. The effects of drift-field distortions, detection properties, and source position on the spatial information were discussed to establish guidelines for the design of PSPCs for specific applications.

Several prototypic PSPCs were constructed and the relations established in this thesis were verified experimentally. Also, the inherent limitations of the RC position encoding method with respect to signal processing time, count-rate capability, and spatial resolution were explored with these prototypic PSPCs.

Since the RC position encoding method represents a powerful technique that will find increasing applications in nuclear physics, medicine, biology, and industry, additional work should be performed to develop a filter that maximizes the ratio of spatial information to spatial uncertainty. Also, methods should be studied to increase the detection efficiency of the PSPCs, because detection efficiency is inversely proportional to the radiation exposure of the object to be

imaged and to the data acquisition time. Attempts should be made to find exact solutions of Eq. (3) to calculate spatial sensitivity, linearity, thermal noise, and errors in the energy-loss and detection-time signals without the approximations introduced by Elmore's definition of rise- and delay time.

LIST OF REFERENCES

LIST OF REFERENCES

1. C. J. Borkowski and M. K. Kopp, "Position-Sensitive Radiation Detector," United States Patent 3,483,377, Dec. 9, 1969.

2. C. J. Borkowski and M. K. Kopp, "New Type of Position-Sensitive Detectors of Ionizing Radiation Using Risetime Measurement," Rev. Sci. Instr. 39, 1515 (1968).

3. R. B. Owen and M. L. Awcock, "One and Two Dimensional Position Sensing Semiconductor Detectors," IEEE Trans. Nucl. Sci. NS-15 (3), 290 (1968).

4. C. J. Borkowski and M. K. Kopp, "Some Applications and Properties of One- and Two-Dimensional Position-Sensitive Proportional Counters," IEEE Trans. Nucl. Sci. NS-17 (3), 340 (1970).

5. C. J. Borkowski and M. K. Kopp, "Position-Sensitive Radiation Detector," United States Patent 3,517,194, June 23, 1970.

6. C. J. Borkowski and M. K. Kopp, "Proportional Counter Photon Camera," IEEE Trans. Nucl. Sci. NS-19 (3), 161 (1972).

7. C. J. Borkowski and M. K. Kopp, "Proportional Counter Radiation Camera," United States Patent 3,786,270, Jan. 15, 1974.

8. C. J. Borkowski, M. K. Kopp, and J. A. Harter, "Line-Scanning Proportional Counter Camera," IEEE Trans. Nucl. Sci. NS-22 (2), 896 (1975).

9. W. R. Kuhlmann, K. H. Lauterjung, B. Schimmer, and K. Sistemich, "Ortsempfindliche Zählrohre," Nucl. Instr. Methods 40, 118 (1966).

10. S. Kalbitzer and W. Melzer, "On the Charge Dividing Mechanism in Position Sensitive Detectors," Nucl. Instr. Methods 56, 301 (1967).

11. L. Kaufman, V. Perez-Mendez, D. Shames, and G. Stoker, "A Multiwire Proportional Chamber for Nuclear Medicine Applications," IEEE Trans. Nucl. Sci. NS-19 (3), 169 (1972).

12. G. Charpak, D. Rahm, and H. Steiner, "Some Developments in the Operation of Multiwire Proportional Chambers," Nucl. Instr. Methods 80, 13 (1969).

13. S. C. Curran and J. D. Craggs, Counting Tubes, Academic Press, Inc., New York, 1949, p. 29.

14. M. K. Kopp, "Wide Band Low Noise Voltage Sensitive Preamplifier with Temperature Compensation," Rev. Sci. Instr. 42, 714 (1971).

15. M. K. Kopp, "Pole-Zero Cancellation in the Feedback Circuit of Wide-Band Preamplifiers to Improve the Baseline Stability for High Count Rates or Large Signals," accepted for publication in Rev. Sci. Instr., August 1975.

16. D. Starner, "Transient Response of some Distributed Parameter Configurations," Lockheed Missiles and Space Division, Sunnyvale, California, Report LMSD-703095, 1960.

17. C. H. Nowlin, "Pulse Shaping for Nuclear Pulse Amplifiers," IEEE Trans. Nucl. Sci. NS-17 (1), 226 (1970).

18. C. H. Nowlin, "Pulse Shaping for Nuclear Pulse Amplifiers (Erratum)," IEEE Trans. Nucl. Sci. NS-18 (6), 456 (1971).

19. W. C. Elmore and M. Sands, Electronics, McGraw-Hill Book Company, Inc., New York, 1949, p. 136.

20. E. Fairstein and J. Hahn, "Nuclear Pulse Amplifiers—Fundamentals and Design Practice," Nucleonics 23 (7), 56 (1965).

21. C. H. Nowlin, Oak Ridge National Laboratory, Oak Ridge, Tennessee, private communication.

22. G. T. Webb, "A Transistor Crossover Pickoff Circuit for Use in Fast-Slow Coincidence Systems," The University of Tennessee, Department of Electrical Engineering, Scientific Report No. 1, Sept. 11, 1961.

23. J. Millman and H. Taub, Pulse, Digital, and Switching Waveforms, McGraw-Hill Book Company, Inc., New York, 1965.

24. H. Nyquist, "Thermal Agitation of Electric Charge in Conductors," Phys. Rev. 32, 110 (1928).

25. R. G. Brown and J. W. Nilsson, Introduction to Linear Systems Analysis, John Wiley and Sons, Inc., New York, 1962, p. 343.

26. R. S. Booth, M. K. Kopp, G. L. Timm, and J. E. Swander, Unfolding Spatial Images from a Position-Sensitive Proportional Neutron Counter, ORNL-TM-4547 (June 1974).

27. Method suggested by C. H. Nowlin, ORNL.

28. T. V. Blalock, The University of Tennessee, Knoxville, Tennessee, private communication.

29. B. G. Harvey et al., "A Spectrometer Focal Plane Detector for Heavy Ions," Nucl. Instr. Methods 104, 21 (1972).

30. J. L. Ford, Jr., P. H. Stelson, and R. L. Robinson, "A Position Sensitive Proportional Detector for a Magnetic Spectrograph," Nucl. Instr. Methods 98, 199 (1972).

31. Y. Dupont et al., "Use of a New Detector for X-ray Diffraction and Kinetics of the Ordering of the Lipids in E. coli Membranes and Model Systems," Nature 238, 331 (1972).

32. J. W. Cable, Oak Ridge National Laboratory, Oak Ridge, Tennessee, private communication.

33. K. L. Swinth and J. C. Crowe, "A Position Sensitive Proportional Counter for Neutron Radiography," IEEE Trans. Nucl. Sci. NS-19 (1), 366 (1972).

34. R. N. St. Onge, "A High Resolution, High Efficiency Proportional Counter X-Ray Camera," IEEE Trans. Nucl. Sci. NS-20 (1), 333 (1973).

35. R. W. Hendricks, Oak Ridge National Laboratory, Oak Ridge, Tennessee, private communication.

36. H. A. Mook, Oak Ridge National Laboratory, Oak Ridge, Tennessee, private communication.

37. P. Gorenstein et al., "Large Area Soft X-Ray Imaging System for Cosmic X-Ray Studies from Rockets," IEEE Trans. Nucl. Sci. NS-22 (1), 616 (1975).

VITA

Manfred Kurt Kopp was born in Koenigsberg, Prussia, Germany, on March 8, 1932. He attended elementary school in that city. In 1945 his family moved to Schwerin, Germany, and in 1948 to Alfeld-Leine, Germany. He attended high school in both cities. In 1950 his family emigrated to Buenos Aires, Argentina. In 1955 he graduated from San Isidro High School in that city and entered the University of Buenos Aires in June 1955, where he received an equivalent Bachelor of Science degree in Electrical Engineering.

From 1956 to 1967 he was employed with the Comision Nacional de Energia Atomica of Buenos Aires, Argentina, as an electrical engineer responsible for the development of instrumentation for the application of radioisotopes in industry. In 1962 he was awarded a fellowship from the International Atomic Energy Agency, Vienna, Austria, to work with C. J. Borkowski, Director of the Instrumentation and Controls Division of ORNL, Oak Ridge, Tennessee.

Since his return to the United States in 1967 he has been employed by the Union Carbide Corporation as a development engineer for the United States Atomic Energy Commission in the Basic Measurement Science Group of the Instrumentation and Controls Division of ORNL.

In 1967 he entered The University of Tennessee, and received a Bachelor of Science degree in Electrical Engineering in 1970. In 1972 he was admitted as a citizen of the United States of America.

He is married to the former Margarita Schmidt of Puerto Bemberg, Argentina. They have one son, Daniel Manfredo, who presently attends the Oak Ridge High School.